Cell Reports

Article

Tumor-specific CD4 T cells instruct monocyte fate in pancreatic ductal adenocarcinoma

Graphical abstract

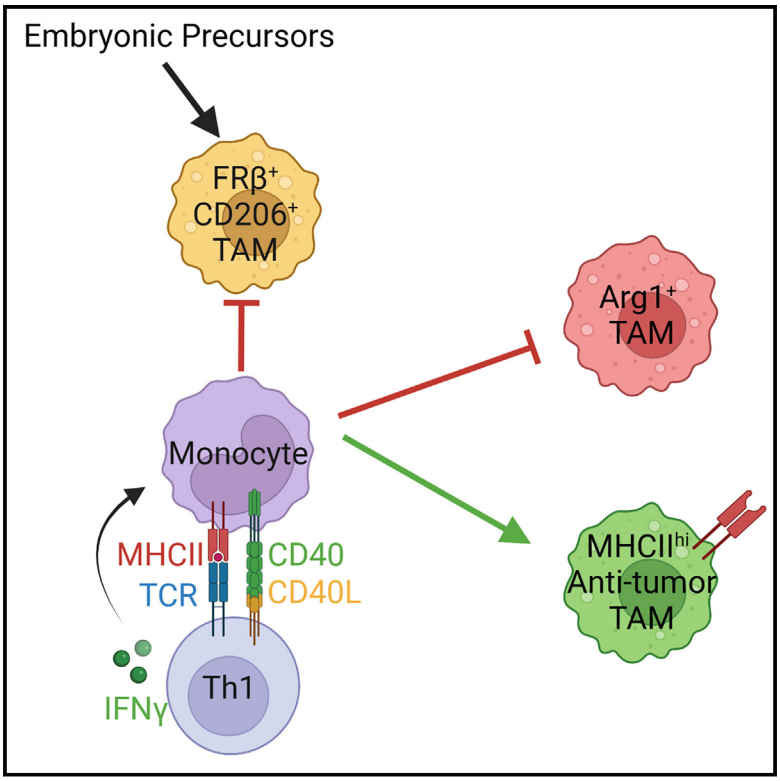

Authors

Michael T. Patterson, Adam L. Burrack, Yingzheng Xu, ..., Konstantin Zaitsev, Jesse W. Williams, Ingunn M. Stromnes

Correspondence

jww@umn.edu (J.W.W.), ingunn@umn.edu (I.M.S.)

In brief

Patterson et al. demonstrate monocyte differentiation into heterogeneous macrophage populations in pancreatic cancer. They identify that tumor-specific CD4 T cells instruct MHCII^{hi} anti-tumor macrophage differentiation through CD40 and IFNγ. Loss of CD4 T cells or MHC class II on monocyte-derived macrophages drives monocytes toward alternatively activated states and promotes tumor growth.

Highlights

- Monocytes are progenitors to most heterogeneous macrophage subsets in PDA
- Tumor-specific CD4 T cells drive anti-tumor MHCII^{hi} macrophages
- Loss of MHC class II on monocyte-derived macrophages promotes tumor progression
- IFNγ and CD40 are non-redundant drivers of MHCII^{hi} antitumor macrophages

Patterson et al., 2023, Cell Reports *42*, 112732
July 25, 2023
https://doi.org/10.1016/j.celrep.2023.112732

CellPress

Cell Reports

CellPress
OPEN ACCESS

Article

Tumor-specific CD4 T cells instruct monocyte fate in pancreatic ductal adenocarcinoma

Michael T. Patterson,[1,2] Adam L. Burrack,[1,3] Yingzheng Xu,[1,2] Grant H. Hickok,[1,3] Zoe C. Schmiechen,[1,3] Samuel Becker,[1,3] Eduardo Cruz-Hinojoza,[1,3] Patricia R. Schrank,[1,2] Ainsley E. Kennedy,[1,2] Maria M. Firulyova,[4,5] Ebony A. Miller,[1,3] Konstantin Zaitsev,[4] Jesse W. Williams,[1,2,*] and Ingunn M. Stromnes[1,3,6,7,8,*]

[1]Center for Immunology, University of Minnesota, Minneapolis, MN 55414, USA
[2]Department of Integrative Biology and Physiology, University of Minnesota, Minneapolis, MN 55414, USA
[3]Department of Microbiology and Immunology, University of Minnesota, Minneapolis, MN 55414, USA
[4]Computer Technologies Laboratory, ITMO University, Saint-Petersburg, Russia
[5]National Medical Research Center, Saint-Petersburg, Russia
[6]Masonic Cancer Center and University of Minnesota Medical School, Minneapolis, MN 55414, USA
[7]Center for Genome Engineering, University of Minnesota Medical School, Minneapolis, MN 55414, USA
[8]Lead contact
*Correspondence: jww@umn.edu (J.W.W.), ingunn@umn.edu (I.M.S.)
https://doi.org/10.1016/j.celrep.2023.112732

SUMMARY

Pancreatic ductal adenocarcinoma (PDA) orchestrates a suppressive tumor microenvironment that fosters immunotherapy resistance. Tumor-associated macrophages (TAMs) are the principal immune cell infiltrating PDA and are heterogeneous. Here, by employing macrophage fate-mapping approaches and single-cell RNA sequencing, we show that monocytes give rise to most macrophage subsets in PDA. Tumor-specific CD4, but not CD8, T cells promote monocyte differentiation into MHCII^{hi} anti-tumor macrophages. By conditional major histocompatibility complex (MHC) class II deletion on monocyte-derived macrophages, we show that tumor antigen presentation is required for instructing monocyte differentiation into anti-tumor macrophages, promoting Th1 cells, abrogating Treg cells, and mitigating CD8 T cell exhaustion. Non-redundant IFNγ and CD40 promote MHCII^{hi} anti-tumor macrophages. Intratumoral monocytes adopt a pro-tumor fate indistinguishable from that of tissue-resident macrophages following loss of macrophage MHC class II or tumor-specific CD4 T cells. Thus, tumor antigen presentation by macrophages to CD4 T cells dictates TAM fate and is a major determinant of macrophage heterogeneity in cancer.

INTRODUCTION

Pancreatic ductal adenocarcinoma (PDA) is a lethal malignancy that resists current treatments.[1] PDA orchestrates a suppressive and fibroinflammatory tumor microenvironment (TME) comprising numerous immune cells.[2] The pancreatic TME interferes with the efficacy of chemotherapy[3] and immunotherapy.[2] However, stromal composition, including particular subsets of T cells and macrophages, correlates with disease-free and overall survival,[4–7] supporting the idea that some aspects of the stromal response may be beneficial.

Pancreatic tumor cells produce numerous pro-myeloid factors, thereby promoting myeloid cell expansion and recruitment into the TME.[2,8–12] Tumor-associated macrophages (TAMs) are abundant cells in PDA and often outnumber tumor cells.[13] While TAM crosstalk with tumor cells and fibroblasts has a pivotal role in promoting carcinogenesis,[14,15] the bidirectional interactions between TAMs and T cells that affect tumor growth are just beginning to be understood.[16,17] In human PDA, TAMs colocalize with T cells, and tumors with an abundant T cell infiltrate also contain numerous TAMs.[13] These data are consistent with an immunogenic subtype that constitutes a large fraction of the patient population.[18]

TAMs are diverse and participate in complex processes, including angiogenesis, metastasis, and inflammation.[19,20] Circulating monocytes and embryonically seeded tissue-resident macrophages comprise the TAM pool.[21–23] Macrophages derived from monocytes display both phenotypic and functional differences compared with tissue-resident TAMs, suggesting that ontogeny may partially account for heterogeneity.[22,24] Tissue-resident TAMs promote extracellular matrix (ECM) deposition, whereas monocyte-derived macrophages act by shaping immunity.[24] In the absence of a defined tumor-specific antigen, TAMs potently suppress T cell activation,[8] and global TAM depletion using Csf1r blockade can be beneficial.[25,26] In contrast, TAM depletion is not advantageous when a tumor-specific T cell response is engaged.[26] Global TAM depletion also fails to promote engineered T cell functionality in autochthonous PDA.[27] While clinical efforts to ablate TAMs have not shown benefit in PDA patients,[28] promoting anti-tumor macrophages using CD40 agonist can exert transient anti-tumor effects.[29] Together, TAMs may aid in antigen-specific T cell-mediated

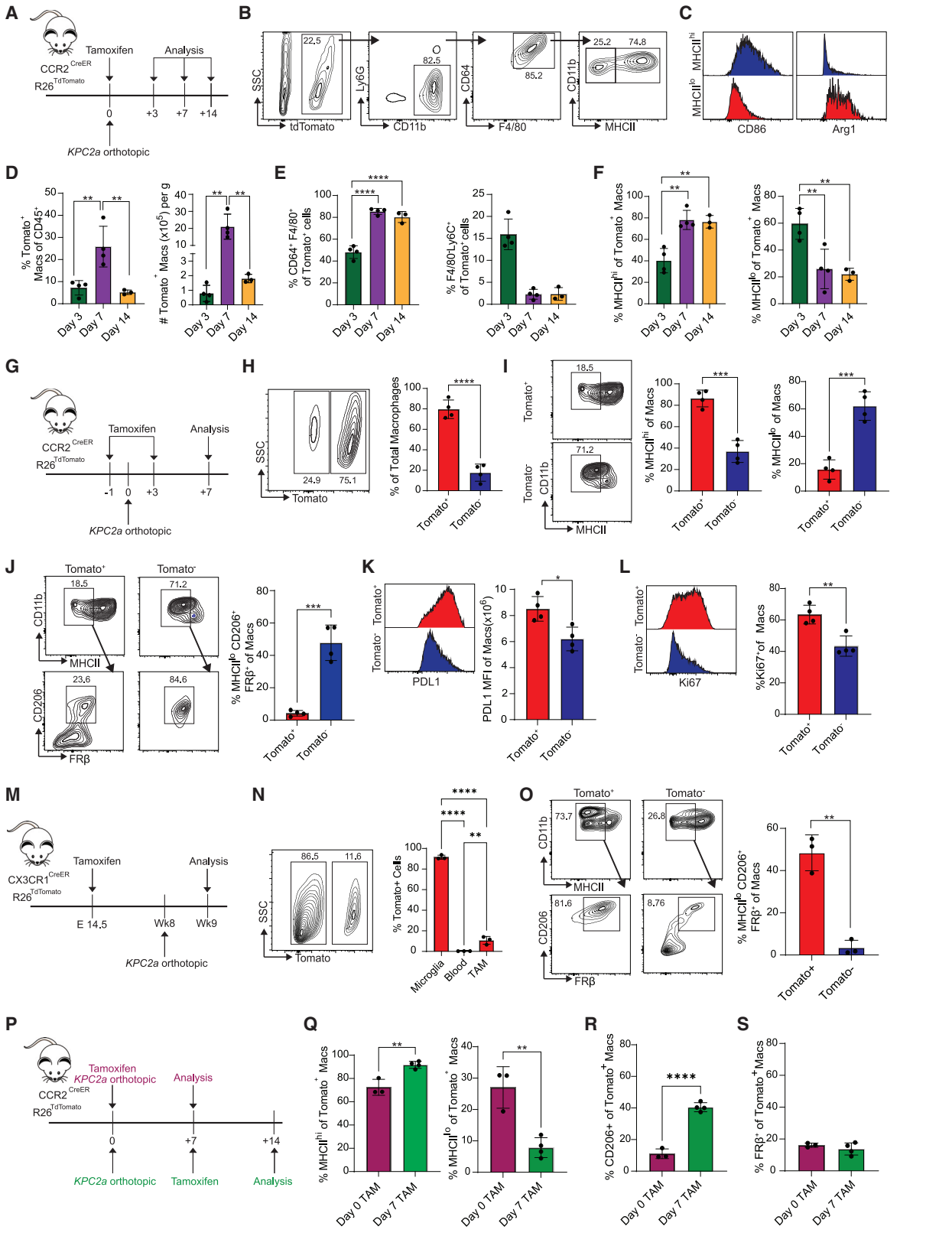

(legend on next page)

destruction of tumors if programmed appropriately. Thus, understanding events that program TAMs toward anti-tumor states could reveal novel therapeutic opportunities.

Here, using an *in vivo* monocyte fate-mapping approach, we temporally track monocyte differentiation in an orthotopic PDA mouse model that expresses a defined model neoantigen.[30] Our study uncovers a critical role for monocyte-derived macrophage cognate tumor antigen presentation to CD4 T cells that dictates macrophage fate and tumor control. Deletion of major histocompatibility complex (MHC) class II in specifically monocyte-derived macrophages or loss of tumor-specific CD4 T cells drives monocytes to adopt a phenotypic and transcriptional state mirroring immunosuppressive pancreas tissue-resident macrophages. We posit that therapeutic resistance by poorly immunogenic tumors may derive from a *de facto* monocyte differentiation trajectory toward a pro-tumor state due to a failure to encounter tumor-specific CD4 T cells.

RESULTS

Fate mapping of monocyte-derived or tissue-resident macrophages in PDA

Given that both monocyte-derived and embryonically derived macrophages contribute to the TAM pool, distinguishing monocyte-derived macrophages *in vivo* has been challenging. Thus, we utilized the CCR2^{CreER} R26^{Tdtomato} mouse, which allows for specific labeling of individual waves of blood monocytes following tamoxifen treatment, enabling tracking of their differentiation upon entry into tissue.[31–33] Tamoxifen treatment of CCR2^{CreER} R26^{Tdtomato} mice revealed robust classical monocyte labeling in the blood, but no labeling of pancreatic tissue-resident macrophages (Figures S1A–S1D), consistent with a reported lack of Ccr2.[34] To track monocyte differentiation in PDA in the presence of tumor-specific T cells, we orthotopically implanted *KPC2a* tumor cells that express a model neoantigen click beetle red luciferase (CB)[30] into the pancreas of CCR2^{CreER} R26^{Tdtomato} mice following a single dose of tamoxifen (Figure 1A). We analyzed mice at days 3, 7, and 14 after implantation and identified two distinct Tomato$^+$ monocyte-derived macrophage subsets based on MHCII^{hi} and MHCII^{lo} expression (Figure 1B). MHCII^{hi} macrophages expressed higher CD86, consistent with an immunostimulatory phenotype, whereas MHCII^{lo} macrophages expressed alternative activation markers, including Arg-1 (Figure 1C). Intratumoral Tomato$^+$ macrophages increased between days 3 and 7 and then decreased by day 14 (Figure 1D), consistent with replacement by subsequent monocyte waves. On day 3, most Tomato$^+$ cells resembled undifferentiated monocytes (CD11b$^+$Ly6C$^+$F4/80$^-$). However, by days 7 and 14, most Tomato$^+$ cells expressed markers of differentiated macrophages (Figure 1E), indicating that recruited monocytes differentiate into macrophages as early as day 7 and are maintained for at least 1 week. At day 3, Tomato$^+$ macrophages (CD64$^+$F480$^+$Ly6C$^-$) were MHCII^{lo}, whereas by days 7 and 14, most Tomato$^+$ macrophages were MHCII^{hi} (Figure 1F) Thus,

Figure 1. Fate mapping of monocyte-derived or tissue-resident macrophages in PDA

(A) *In vivo* monocyte tracking approach in CCR2^{CreER} R26^{TdTomato} mice orthotopically implanted with *KPC2a* tumor cells and treated with tamoxifen. See also Figure S1.

(B) Gating strategy for Tomato$^+$ MHCII^{hi} and MHCII^{lo} macrophages.

(C) Representative CD86 and Arg1 histograms gated on Tomato$^+$ MHCII^{hi} or MHCII^{lo} TAMs.

(D) Frequency and number of Tomato$^+$ TAMs. Each dot is an independent mouse. Data are mean ± SEM; n = 3–4 mice per group; **p < 0.005; one-way ANOVA with Tukey's posttest.

(E) Proportion of intratumoral Tomato$^+$ cells that are macrophages (CD64$^+$F4/80$^+$) or monocytes (F4/80$^-$Ly6C$^+$). Each dot is an independent mouse. Data are mean ± SEM; n = 3–4 mice per group; ****p < 0.0001; one-way ANOVA with Tukey's posttest.

(F) Proportion of intratumoral Tomato$^+$ MHCII^{hi} or MHCII^{lo} macrophages. Each dot is an independent mouse. Data are mean ± SEM; n = 3–4 mice per group; **p < 0.005; one-way ANOVA with Tukey's posttest.

(G) *In vivo* monocyte tracking approach in CCR2^{CreER} R26^{TdTomato} mice implanted with *KPC2a* tumor cells and treated with tamoxifen twice.

(H) Representative plot gated on intratumoral F4/80$^+$CD64$^+$ macrophages on day 7. Proportion of total Tomato$^+$ macrophages. Each dot is an independent mouse. Data are mean ± SEM; n = 4 mice per group; ****p < 0.0001; Student's t test.

(I) Representative plots gated on day 7 and proportion of Tomato$^+$ or Tomato$^-$ intratumoral MHCII^{hi} or MHCII^{lo} macrophages on day 7. Each dot is an independent mouse. Data are mean ± SEM; n = 4 mice per group; ***p < 0.001; Student's t test.

(J) Representative plots gated on day 7 and proportion of Tomato$^+$ and Tomato$^-$ MHCII^{lo}CD206$^+$FRβ$^+$ macrophages on day 7. Each dot is an independent mouse. Data are mean ± SEM; n = 4 mice per group; ***p < 0.001; Student's t test.

(K) PD-L1 staining and mean fluorescence intensity (MFI) of Tomato$^+$ and Tomato$^-$ macrophages at day 7. Each dot is an independent mouse. Data are mean ± SEM; n = 4 mice per group; *p < 0.05; Student's t test.

(L) Representative histograms and frequency of Ki67$^+$ macrophages on day 7. Each dot is an independent mouse. Data are mean ± SEM; n = 4 mice per group; **p < 0.005; Student's t test.

(M) Embryonic fate-mapping approach in CX3CR1^{CreER} R26^{TdTomato}. Briefly, pregnant mothers were gavaged with tamoxifen on embryonic day 14.5 and then progeny were implanted with tumors. See also Figure S2.

(N) Representative plot gated on intratumoral F4/80$^+$CD64$^+$ macrophages on day 7 from (M). Proportion of each cell subtype that is Tomato$^+$ is shown. Each dot is an independent mouse. Data are mean ± SEM; n = 3 mice per group; **p < 0.005, ****p < 0.0001; one-way ANOVA with Tukey's post test.

(O) Representative plots gated on day 7 and proportion of Tomato$^+$ and Tomato$^-$ MHCII^{lo}CD206$^+$FRβ$^+$ tumor macrophages. Each dot is an independent mouse. Data are mean ± SEM; n = 3 mice per group; **p < 0.005; Student's t test.

(P) Experimental schematic to label the initial wave of recruited monocytes (purple) or subsequent waves of recruited monocytes (green).

(Q) Proportion of each monocyte wave that gives rise to MHCII^{hi} or MHCII^{lo} macrophages. Each dot is an independent mouse. Data are mean ± SEM; n = 3–4 mice per group; **p < 0.005; Student's t test.

(R) Proportion of each monocyte wave that gives rise to CD206$^+$ macrophages. Each dot is an independent mouse. Data are mean ± SEM; n = 3–4 mice per group; ****p < 0.0001; Student's t test.

(S) Proportion of each monocyte wave that gives rise to FRβ$^+$ macrophages. Each dot is an independent mouse. Data are mean ± SEM; n = 3–4 mice per group.

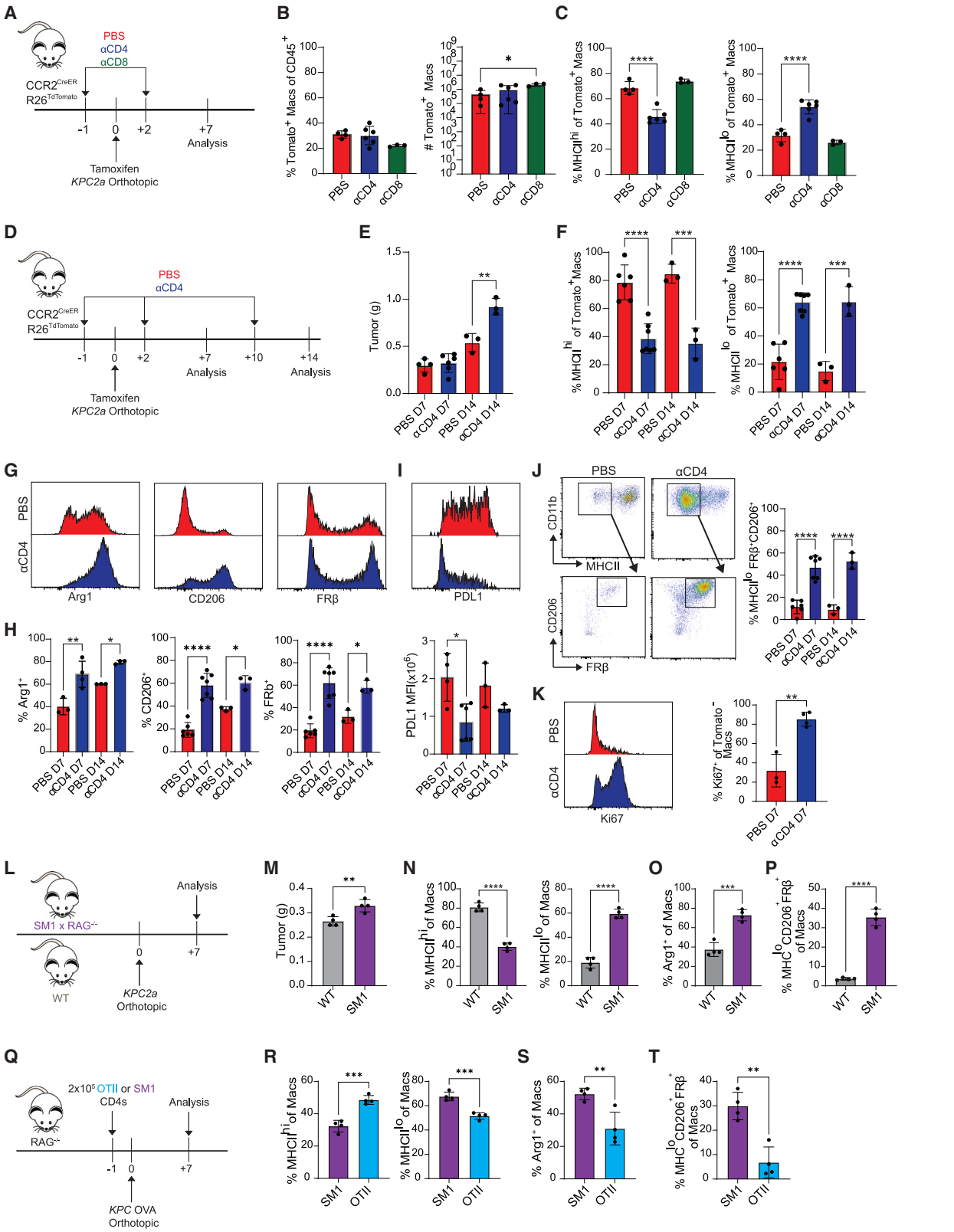

(legend on next page)

monocytes undergo an initial differentiation into a transitory MHCII^{lo} state and progressively upregulate MHCII. Alternatively, MHCII^{hi} monocyte-derived macrophages may preferentially expand during tumor progression.

We next compared the phenotype of Tomato^{+} monocyte-derived macrophages with that of Tomato^{-} tissue-resident macrophages. We administered tamoxifen at both prior to and following tumor implantation (Figure 1G), which resulted in complete monocyte labeling for 7 days (Figure S1E) and resulting in 80% of TAMs that were Tomato^{+} (Figure 1H). Consistent with a prior report,[24] non-monocyte-derived TAMs primarily adopted an MHCII^{lo} phenotype (Figure 1I). MHCII^{lo} Tomato^{-} macrophages also expressed markers of alternative activation including CD206 and FRβ. In contrast, Tomato^{+} macrophages rarely adopted a MHCII^{lo}CD206^{+}FRβ^{+} phenotype (Figure 1J) and instead expressed high PD-L1 (Figure 1K) and were proliferative (Figure 1L). Macrophages in healthy pancreas were also MHCII^{lo}CD206^{+}FRβ^{+} (Figures S2A and S2B). These data highlight immune modulatory and proliferation differences based on macrophage ontogeny. To investigate the developmental origin of pancreatic tissue-resident macrophages in PDA, we performed embryonic pulse-chase experiments in tumor-bearing CX3CR1^{CreER} R26^{TdTomato} mice. Given that CX3CR1 is turned on in embryonic-derived macrophages during development,[35] *in utero* treatment of tamoxifen allows for specific labeling of embryonic macrophages.[32] Pregnant CX3CR1^{CreER} R26^{TdTomato} mice were administered tamoxifen on embryonic day 14.5 and then their progeny were implanted with tumors and assessed 7 days after (Figure 1M). Nearly 100% of microglia were Tomato^{+}, while labeling in the blood was negligible (Figure 1N), validating the specificity of this approach. Approximately 10% of TAMs were Tomato^{+} (Figure 1N), confirming that most TAMs are of monocytic origin. Tomato^{+} TAMs primarily adopted an MHCII^{lo}CD206^{+}FRβ^{+} phenotype, while a much lower frequency of Tomato^{-} TAMs adopted this phenotype (Figure 1O).

We next compared monocyte-derived macrophage fate during early invasive tumor growth with monocytes recruited at a later time point (Figure 1P). Monocytes recruited later during tumor growth preferentially differentiated into MHCII^{hi} macrophages compared with initially recruited monocytes (Figure 1Q). For monocytes in larger tumors, a subset upregulated CD206 (Figure 1R), suggesting acquisition of an alternatively activated phenotype. At both time points, Tomato^{+} macrophages failed to upregulate FRβ (Figure 1S). Together, the data support that monocytes comprise most TAMs in neoantigen+ PDA and that the MHCII^{lo}CD206^{+}FRβ^{+} phenotype may identify pancreas-resident macrophages.

CD4 T cells govern fate decisions in tumor-infiltrating monocytes

T cells colocalize with macrophages in resected human PDA,[13] and engineered T cell therapy recruits monocytes into *KPC* PDA.[27] Given these observations, we hypothesized that T cells may instruct monocyte differentiation. Therefore, we depleted CD4 or CD8 T cells in CCR2^{creER} R26^{tdTomato} mice bearing orthotopic tumors and assessed monocyte differentiation at day 7 (Figure 2A). CD8 T cell depletion led to a modest but significant increase in number of Tomato^{+} macrophages (Figure 2B), suggesting regulation of monocyte recruitment and/or survival. While CD8 T cell depletion had minimal effect on the Tomato^{+} macrophage phenotype, CD4 T cell depletion led to a dramatic reduction in MHCII^{hi} macrophages and a corresponding

Figure 2. CD4 T cells govern fate decisions of tumor-infiltrating monocytes

(A) Experimental approach to test the role of T cell subsets on monocyte fate.

(B) Proportion (left) and number (right) of Tomato^{+} intratumoral macrophages. Each dot is an independent mouse. Data are mean ± SEM; n = 3–5 mice per group; *p < 0.05; one-way ANOVA with Tukey's posttest.

(C) Proportion of MHCII^{hi} or MHCII^{lo} Tomato^{+} macrophages. Each dot is an independent mouse. Data are mean ± SEM; n = 3–5 mice per group; ****p < 0.0001; one-way ANOVA with Tukey's posttest.

(D) Experimental approach to test the impact of prolonged CD4 T cell depletion in tumor-bearing CCR2^{CreER} R26^{TdTomato} mice. See also Figure S3.

(E) Tumor weight from mice in (D); n = 3–6 mice per group. Data are mean ± SEM; **p < 0.005; Student's t test for each time point.

(F) Proportion of Tomato^{+} macrophages from (D) that are MHCII^{hi} or MHCII^{lo}. Data are mean ± SEM; n = 3–6 mice per group; ***p < 0.001, ****p < 0.0001; Student's t test for each time point.

(G) Representative histograms gated on Tomato^{+} macrophages isolated from PBS- or αCD4-treated mice.

(H) Proportion of Tomato^{+} macrophages expressing Arg1, CD206, and FRβ from PBS- or αCD4-treated mice. Data are mean ± SEM; n = 3–6 mice per group; *p < 0.05, **p < 0.005, ****p < 0.0001; Student's t test for each time point.

(I) Representative PD-L1 staining (top) and MFI of Tomato^{+} macrophages from PBS- or αCD4-treated mice (bottom); n = 3–6 mice per group; *p < 0.05; Student's t test.

(J) Representative plots and proportion of Tomato^{+} MHCII^{lo} macrophages that coexpress CD206 and FRβ from mice in (D). Data are mean ± SEM; n = 3–6 mice per group; ****p < 0.0001; Student's t test for each time point.

(K) Representative histograms and proportion of Tomato^{-} macrophages that are Ki67^{+}. Data are mean ± SEM; n = 3–4 mice per group; **p < 0.005; Student's t test.

(L) Experimental approach to test the impact of T cell antigen specificity on monocyte differentiation. See also Figures S4A–S4F.

(M) Tumor weight from (L). Data are mean ± SEM; n = 4 mice per group; **p < 0.005; Student's t test.

(N) Proportion of MHCII^{hi} or MHCII^{lo} macrophages from (L). Data are mean ± SEM; n = 4 mice per group; ****p < 0.0001; Student's t test.

(O) Proportion of Arg1^{+} macrophages from (L). Data are mean ± SEM; n = 4 mice per group; ***p < 0.001; Student's t test.

(P) Proportion of MHCII^{lo}CD206^{+}FRβ^{+} macrophages from (L). Data are mean ± SEM; n = 4 mice per group; ****p < 0.0001; Student's t test.

(Q) Experimental approach to test if transferred tumor-specific (OTII) or non-specific (SM1) CD4 T cells modulate monocyte differentiation in KPC-OVA-bearing *Rag*$^{-/-}$ mice. See also Figures S4G–S4I.

(R) Proportion of MHCII^{hi} or MHCII^{lo} macrophages from (Q). Data are mean ± SEM; n = 4 mice per group; ***p < 0.001; Student's t test.

(S) Proportion of Arg1^{+} macrophages from (Q). Data are mean ± SEM; n = 4 mice per group; **p < 0.005; Student's t test.

(T) Proportion of MHCII^{lo}CD206^{+}FRβ^{+} macrophages from (Q). Data are mean ± SEM; n = 4 mice per group; **p < 0.005; Student's t test. See also Figure S5.

increase in MHCII^{lo} macrophages (Figure 2C). In contrast, CD8 T cell depletion did not have an impact on monocyte phenotype at day 7 (Figure 2C) or following extended depletion at day 14 (Figures S3A–S3C). To test if CD4 T cells were merely modulating MHC class II or instead shifting macrophage subsets, we developed an expanded antibody panel to delineate macrophage subpopulations (Figure 2D). At day 14, tumor weights were significantly increased in CD4 T cell-depleted mice compared with control mice, indicating that CD4 T cells control tumor growth (Figure 2E). Moreover, CD4 T cell depletion increased Tomato^{+} MHCII^{lo}, Arg1^{+}, CD206^{+}, and/or FRβ^{+} macrophages (Figures 2F–2H) while decreasing PD-L1 (Figure 2I). Unexpectedly, CD4 T cell depletion biased monocyte-derived macrophages toward an MHCII^{lo}CD206^{+}FRβ^{+} tissue-resident phenotype (Figure 2J). Finally, CD4 T cell depletion increased Tomato^{-} tissue-resident macrophage proliferation (Figure 2K). Thus, CD4 T cells instruct monocytes toward an MHCII^{hi} state and limit differentiation into Arg1^{+} or CD206^{+}FRβ^{+} TAMs, the latter indistinguishable from tissue-resident TAMs.

Tumor-specific CD4 T cells drive MHCII^{hi} macrophage differentiation

To test if T cell antigen specificity affects macrophage differentiation, *KPC*2a cells were implanted into wild-type (WT) or SM1 *Rag1*$^{-/-}$ mice, in which CD4 T cells express a monoclonal T cell receptor (TCR) specific to a *Salmonella* antigen[36] (Figure 2L), thereby eliminating endogenous tumor-reactive T cells. Tumors were larger in SM1 compared with WT mice (Figure 2M). Frequency of intratumoral MHCII^{lo} (Figure 2N), Arg1^{+} (Figure 2O), and MHC^{lo}CD206^{+}FRβ^{+} (Figure 2P) TAMs was also increased in SM1 mice. Intratumoral CD4 T cell number and percentage were not significantly different between WT and SM1 mice (Figures S4A–S4C). However, the frequency of CD4 T cells that expressed T-bet, CD44, or Klrg1 was reduced in SM1 mice (Figures S4D–S4F). To determine if antigen-specific CD4 T cells were sufficient to promote MHCII^{hi} TAMs, tumor-specific OTII or non-specific SM1 CD4 T cells were infused into *Rag1*$^{-/-}$ mice bearing orthotopic *KPC*-OVA tumors (Figure 2Q). OTII cells tended to reduce tumor mass (Figure S4G) and significantly increased MHCII^{hi} TAMs while decreasing Arg1^{+} and MHC^{lo}CD206^{+}FRβ^{+} TAMs (Figures 2R–2T). Intratumoral OTII cells also trended to be increased compared with SM1 T cells (Figures S4H and S4I). CD4 T cell depletion failed to alter the bias toward suppressive TAMs in the neoantigen-negative (CB^{-}) parental *KPC*2 tumors in CCR2^{CreER} R26^{Tdtomato} mice (Figure S5). Thus, tumor-specific CD4 T cells promote monocyte differentiation into MHCII^{hi} TAMs, and in their absence, monocytes default to suppressive states.

MHC class II on monocyte-derived TAMs promotes Th1 CD4 T cells and anti-tumor immunity

To investigate the role of monocyte-derived macrophage antigen presentation in tumors, we generated CCR2^{CreER} MHCII$^{fl/fl}$ mice to conditionally delete MHC class II on monocyte-derived macrophages (Figures 3A and 3B). Loss of MHC class II on monocyte-derived TAMs increased tumor weight and Arg1^{+} and MHC^{lo}CD206^{+}FRβ^{+} TAMs (Figures 3C–3E). Remaining MHCII^{+} TAMs in tamoxifen-treated CCR2^{CreER} MHCII$^{fl/fl}$ mice were MHCII^{lo}CD206^{+}FRβ^{+} tissue-resident phenotype, confirming the targeting approach specificity (Figure S6A). Furthermore, dendritic cell (DC) MHC class II was maintained (Figures S6B and S6C), supporting the specificity of this approach. Loss of MHC class II on monocyte-derived TAMs reduced intratumoral CD4 T cell frequency and number (Figures 3F and 3G) and intratumoral CD8 T cell number (Figure 3H). Strikingly, MHC class II loss on monocyte-derived TAMs also increased T regulatory cell (Treg) frequency (Figure 3I) and decreased T-bet^{+} and IFNγ-producing CD4 T cells (Figures 3J and 3K). Finally, MHC class II loss increased the frequency of CD8 T cells coexpressing PD1 and Lag3 (Figure 3L), markers that identify exhausted T cells[30] and may be a result of increased Treg and/or suppressive TAMs in this context. Thus, MHC class II on monocyte-derived TAMs is critical for promoting anti-tumor Th1 cells and antitumor immunity.

Single-cell fate mapping of monocyte differentiation in PDA

We next sought to interrogate how CD4 T cells affect monocyte differentiation trajectories. We performed single-cell RNA sequencing (scRNA-seq) combined with cellular indexing of transcriptomes and epitopes sequencing (CITE-seq) of sorted CD45^{+}Tomato^{+} and CD45^{+}Tomato^{-} immune cells from orthotopic tumors from control or CD4-depleted CCR2^{CreER} R26$^{Td\ tomato}$ mice (Figure S7A). Given the overlap in phenotype of tumor-infiltrating TAMs following CD4 T cell depletion at days 7 and 14, we selected the day 7 time point because tumor weight was similar (Figure 2E). Control tumors were harvested at days 3 and 7, and CD4 T cell-depleted tumors were harvested at day 7 post monocyte labeling and tumor implantation (Figure S7A). Clustering of integrated data at the two time points revealed distinct immune populations (Figures 4A and S7B). Subclustering of monocyte/macrophage populations revealed five populations (Figure 4B). Cluster 1 was enriched for monocyte-specific genes, including *Ly6c2*, *Ms4a4c*, and *Plac8* (Figure 4C). Clusters 2, 3, and 4 expressed macrophage-specific genes such as *Adgre1, Cd68*, and *Fcgr1*, suggesting three distinct macrophage populations (Figure S8A). Cluster 2 was enriched for *Folr2*, *Lyve1*, and *Cd206* (Figures 4C and S8A), which are elevated in tissue-resident macrophages.[37,38] Cluster 3 was enriched for MHC class II antigen presentation (*H2-Ab1*, *H2-Aa*, *Cd74*), and cluster 4 expressed immunosuppressive genes like *Arg1* and *Spp1* (Figure 4C), mirroring the MHCII^{hi} or MHCII^{lo} Arg-1^{+} populations (Figure 1B). Both Arg1[39] and Spp1[40] have immunosuppressive properties, suggesting pro-tumorigenic functions. Cluster 5 consisted of proliferating cells, as shown by abundant *Mki67* and *Top2a* (Figure 4C). Based on CITE-seq analysis, MHC class II protein was almost exclusively restricted to cluster 3, while FRβ was primarily unique to cluster 2 (Figure 4D). PD-L1 was expressed by both clusters 3 and 4, yet was absent from cluster 2. We next compared gene expression in macrophage clusters with canonical pro-inflammatory or anti-inflammatory macrophage gene sets. Cluster 3 (MHCII^{hi}) expressed more genes associated with a pro-inflammatory state, including IFNγ-inducible chemokine ligands *Cxcl9* and *Cxcl10*. In contrast, cluster 2 (*Folr2*$^{+}$) and cluster 4 (MHCII^{lo} *Arg1*$^{+}$) were enriched for anti-inflammatory genes such as *Il10* (Figure 4E).

We next assessed the relative contribution of monocytes to the TAM pool (Figure S8B). Most Tomato^{-} macrophages

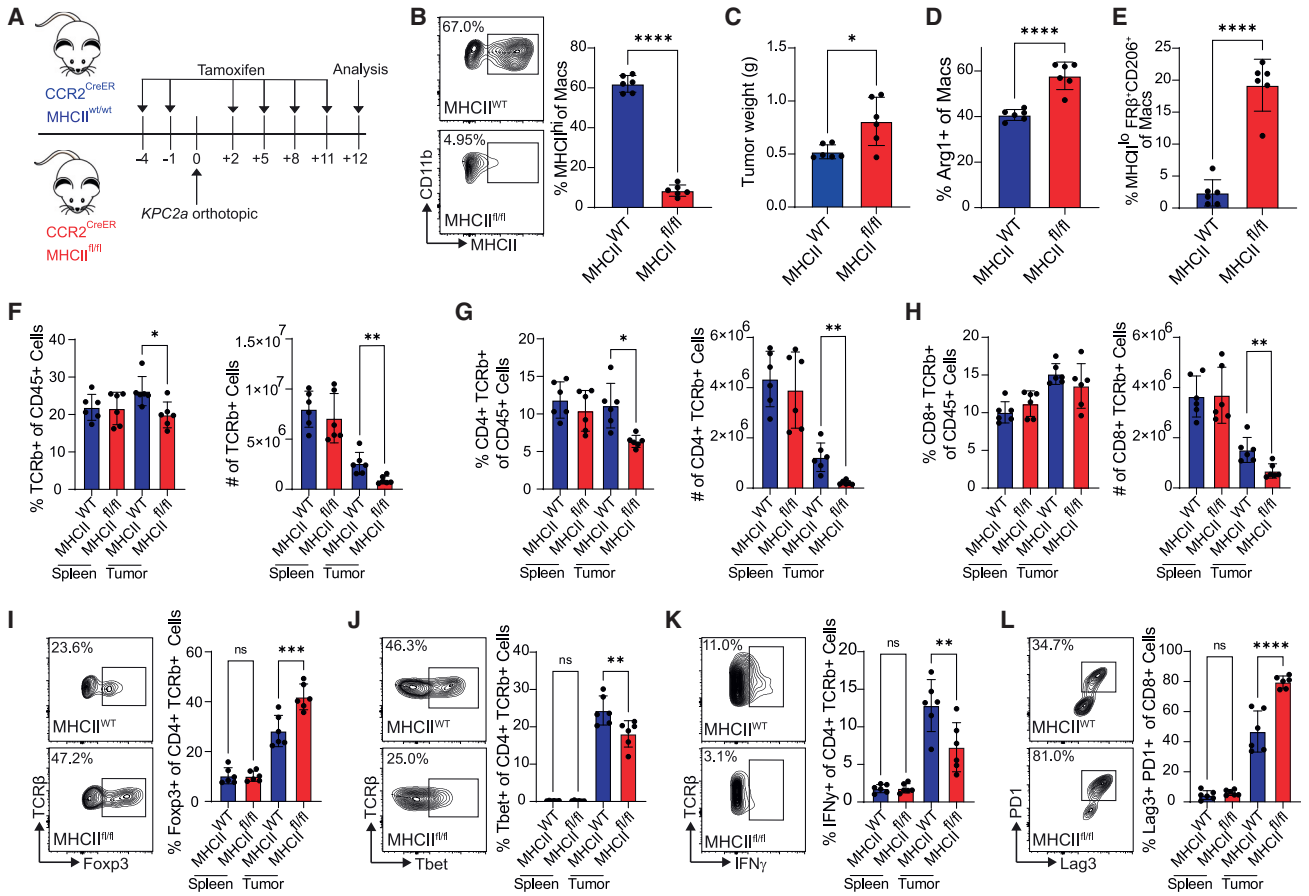

Figure 3. MHC class II on monocyte-derived TAMs promotes Th1 CD4 T cells and anti-tumor immunity

(A) Experimental approach to test the impact of MHC class II deletion in monocyte-derived macrophages. See also Figure S6.

(B) MHC class II staining gated on TAMs at day 12. Data are mean ± SEM; n = 6 mice per group; ****p < 0.0001; Student's t test.

(C) Tumor weights. Data are mean ± SEM; n = 6 mice per group; *p < 0.05; Student's t test.

(D) Proportion of Arg1$^+$ macrophages. Data are mean ± SEM; n = 6 mice per group; ****p < 0.0001; Student's t test.

(E) Proportion of MHCII^{lo}CD206$^+$FRβ$^+$ macrophages. Data are mean ± SEM; n = 6 mice per group; ****p < 0.0001; Student's t test.

(F) Frequency and number of T cells. Data are mean ± SEM; n = 6 mice per group; *p < 0.05, **p < 0.005; Student's t test for each tissue.

(G) Frequency and number of CD4 T cells. Data are mean ± SEM; n = 6 mice per group; *p < 0.05, **p < 0.005; Student's t test for each tissue.

(H) Frequency and number of CD8 T cells. Data are mean ± SEM; n = 6 mice per group; **p < 0.005; Student's t test for each tissue.

(I) Representative Foxp3 staining gated on CD4 T cells and frequency. Data are mean ± SEM; n = 6 mice per group; ***p < 0.001; Student's t test for each tissue.

(J) Frequency of CD4 T cells that are T-bet$^+$. Data are mean ± SEM; n = 6 mice per group; **p < 0.005; Student's t test for each tissue.

(K) Frequency of CD4 T cells producing IFNγ after *ex vivo* restimulation. Data are mean ± SEM; n = 6 mice per group; **p < 0.005, Student's t test for each tissue.

(L) Proportion of CD8 T cells coexpressing Lag3 and PD1. Data are mean ± SEM; n = 6 mice per group; ****p < 0.0001; Student's t test for each tissue.

clustered within the *Folr2*$^+$ cluster, whereas Tomato$^+$ macrophages clustered within the monocyte, MHCII^{hi}, and Arg1$^+$ clusters (Figure 4F). Together, these data support that, at steady state, MHCII^{hi} and Arg1$^+$ macrophages are derived from monocytes, and FRβ$^+$ (*Folr2*$^+$) macrophages are derived from tissue-resident macrophages.

To examine temporal changes, we compared the proportions of each cluster between days 3 and 7. At day 3, most macrophages clustered within the *Folr2*$^+$ or *Arg1*$^+$ population. However, by day 7, macrophages adopting the MHCII^{hi} phenotype increased (Figures 4G and S8C), suggestive of monocyte skewing toward MHCII^{hi} over time (Figure 1F) and corresponding to timing of developing an antigen-specific CD4 T cell response.

CD4 T cell depletion rewires monocyte differentiation toward a pro-tumor state

To further assess the role of CD4 T cells in monocyte fate, we clustered intratumoral Tomato$^+$ cells from control or CD4 T cell-depleted mice. Most Tomato$^+$ cells clustered in the MHCII^{hi} population in tumors from control mice (Figures 5A and 5B). In contrast, CD4 T cell depletion increased Tomato$^+$ cells clustering with the *Arg1*$^+$ or *Folr2*$^+$ population, suggesting acquisition of a pro-tumor macrophage transcriptional profile, while impairing acquisition of an MHCII^{hi} state (Figures 5A and 5B). Furthermore, Tomato$^+$ cells upregulated genes associated with tissue-resident macrophages, including *Lyve1*,[38] in CD4 T cell-depleted tumors (Figure S8D). Using pseudotime,[41] *Folr2*$^+$ macrophages were predicted to be the most terminally

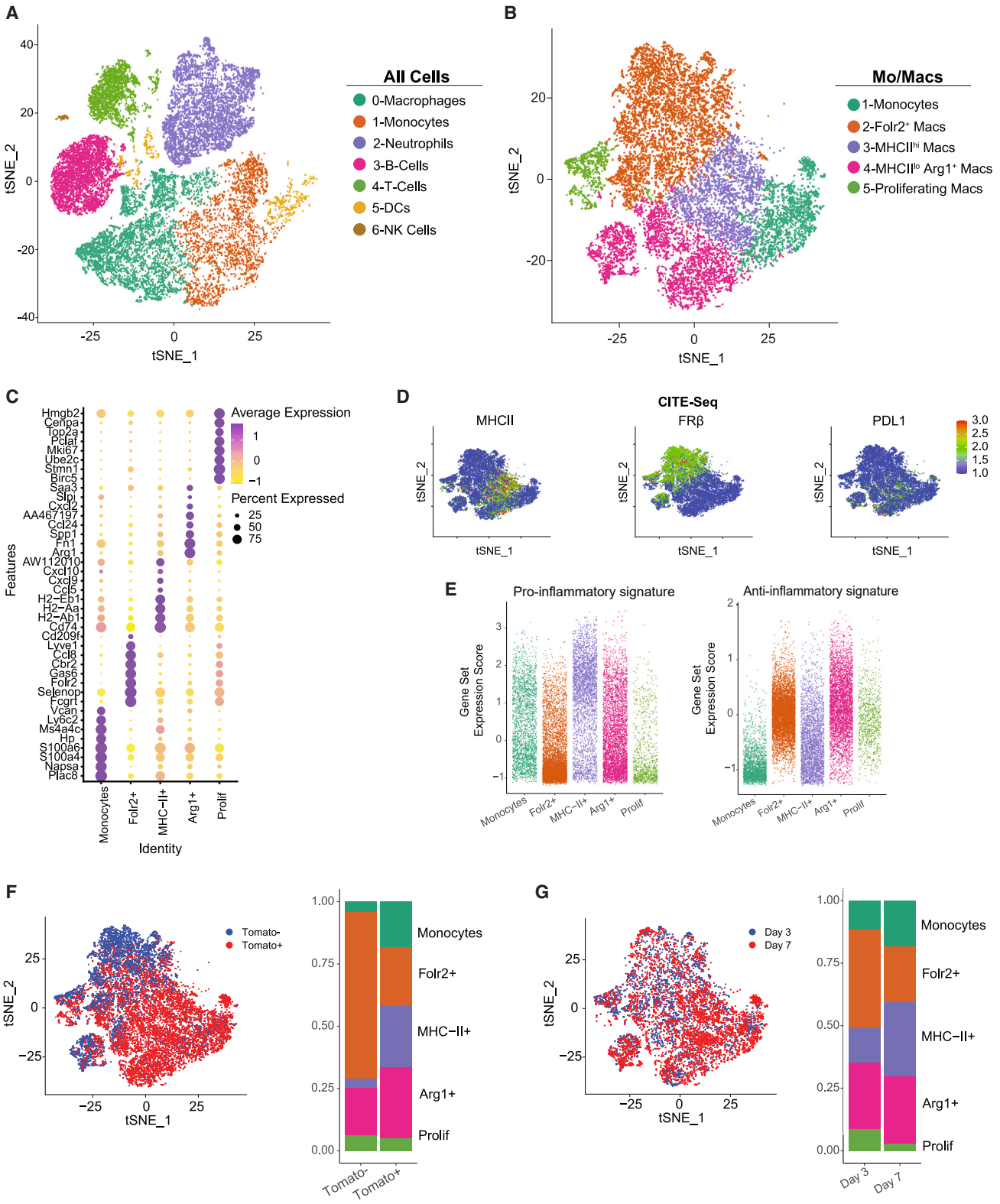

Figure 4. Single-cell fate mapping of monocyte differentiation in PDA

(A) t-distributed stochastic neighbor embedding (t-SNE) plots of intratumoral immune cells isolated on days 3 and 7 ± αCD4 post tumor (n = 4 orthotopic *KPC*2a tumors per group). See also Figure S7.

(legend continued on next page)

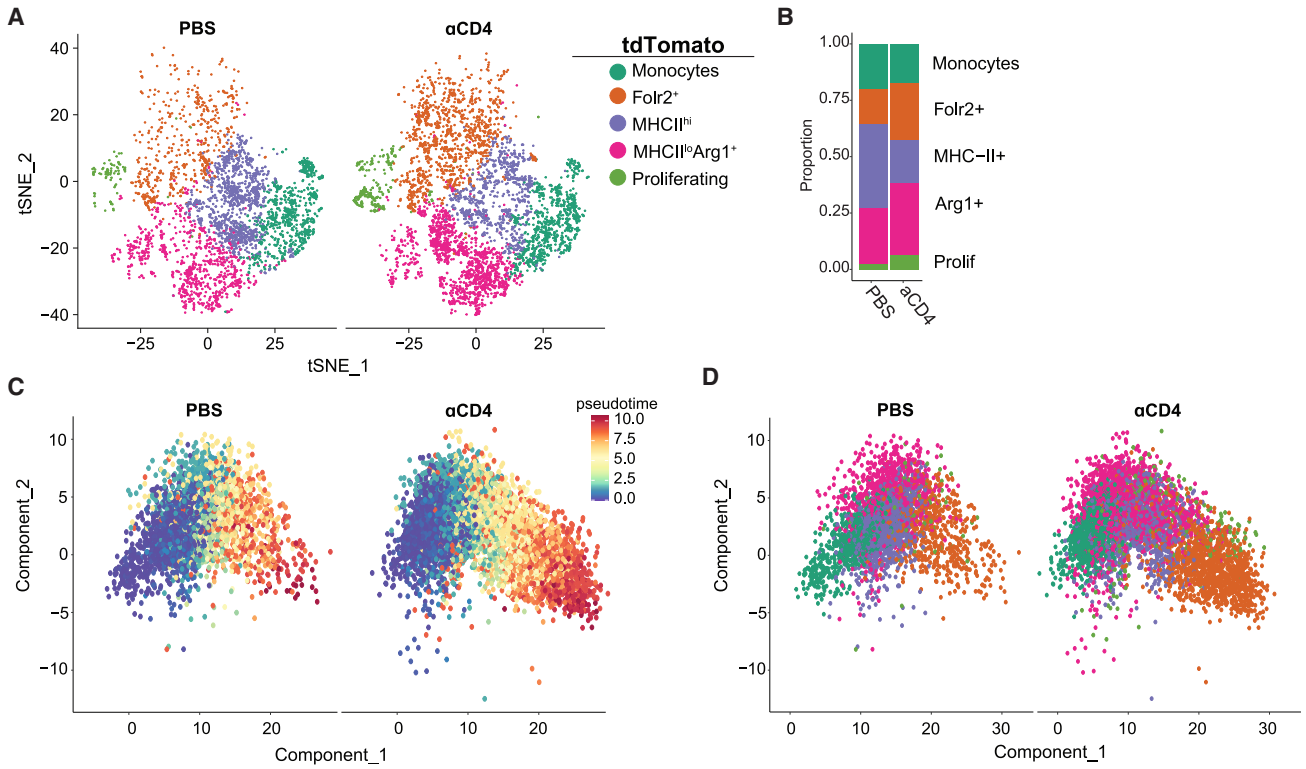

Figure 5. CD4 T cell depletion rewires monocyte differentiation toward a pro-tumor state

(A) t-SNE plot of intratumoral Tomato$^+$ monocytes/macrophages from PBS- or αCD4-treated mice. See also Figure S8D.

(B) Proportion of each cluster among intratumoral Tomato$^+$ monocyte/macrophages from PBS- or αCD4-treated mice.

(C) Pseudotime analysis of Tomato$^+$ monocyte/macrophages split by pseudotime. See also Figure S9.

(D) Pseudotime analysis of Tomato$^+$ monocyte/macrophages split by cluster.

differentiated population (Figures 5C and 5D). In the presence of CD4 T cells, monocytes gave rise to MHCII^{hi} or Arg1$^+$ macrophages. In contrast, CD4 T cell depletion resulted in MHCII^{hi} and Arg1$^+$ macrophages adopting a *Folr2*$^+$ macrophage fate (Figure 5D). Kinetic analysis of cluster-defining genes showed that the upregulation of *Arg1* and *Folr2* was accelerated and *H2-Aa* was blunted in macrophages from CD4 T cell-depleted tumors (Figure S9). Together, the data support that tumor-specific CD4 T cells may halt MHCII^{hi} macrophage transition to a suppressive state.

Ifngr1 and CD40 signaling non-redundantly drive anti-tumor TAM differentiation

We utilized NicheNet[42] to predict downstream ligand gene interactions driving anti-tumor TAM fate. By setting CD4 T cells as the donor cluster and MHCII^{hi} macrophages as the acceptor cluster, several predicted ligand-gene interactions, including *Ifng*, *Tnf*, and *Cd40l*, that may drive MHCII^{hi} macrophage differentiation were identified (Figure 6A). Both IFNγ and CD40L promote anti-tumor immunity[43] and may be more highly expressed by CD4 T cells rather than CD8 T cells, in *KPC*2a tumors (Figure S10). MHCII^{hi} macrophages exhibited increased *Stat1* compared with MHCII^{lo} macrophages (Figure 6B), consistent with enhanced downstream IFNγR signaling.[44] *Ifngr1*$^{-/-}$ mice had significantly larger tumors at day 14 (Figure 6C) that correlated with expanded MHCII^{lo} and decreased MHCII^{hi} TAMs (Figure 6D). As predicted from NicheNet, tumors from *Ifngr1*$^{-/-}$ mice displayed an expansion of Arg1$^+$ TAMs (Figure 6E) and MHCII^{lo}CD206$^+$FRβ$^+$ TAMs compared with tumors from WT mice (Figure 6F), suggesting that IFNγR signaling mediates TAM fate decision toward an anti-tumor state. Contradictory to other models,[45,46] PD-L1 was unchanged at day 7 and only slightly reduced at day 14 in *Ifngr1*$^{-/-}$ mice (Figure 6G), indicating IFNγR-independent mechanisms for driving PD-L1.

(B) t-SNE plots of only monocytes and macrophage clusters.

(C) Heatmap showing normalized cluster-specific gene expression. See also Figure S8A.

(D) Normalized CITE-seq protein in t-SNE plot.

(E) Gene set enrichment analysis of canonical pro-inflammatory and anti-inflammatory genes split by monocyte/macrophage cluster defined in (B).

(F) t-SNE plot showing Tomato$^+$ and Tomato$^-$ cells from days 3 and 7 untreated, and proportion of each monocyte/macrophage cluster among Tomato$^+$ and Tomato$^-$ myeloid cells from clusters defined in (B). See also Figure S8B.

(G) t-SNE plot and proportion of each monocyte/macrophage cluster at days 3 and 7. See also Figure S8C.

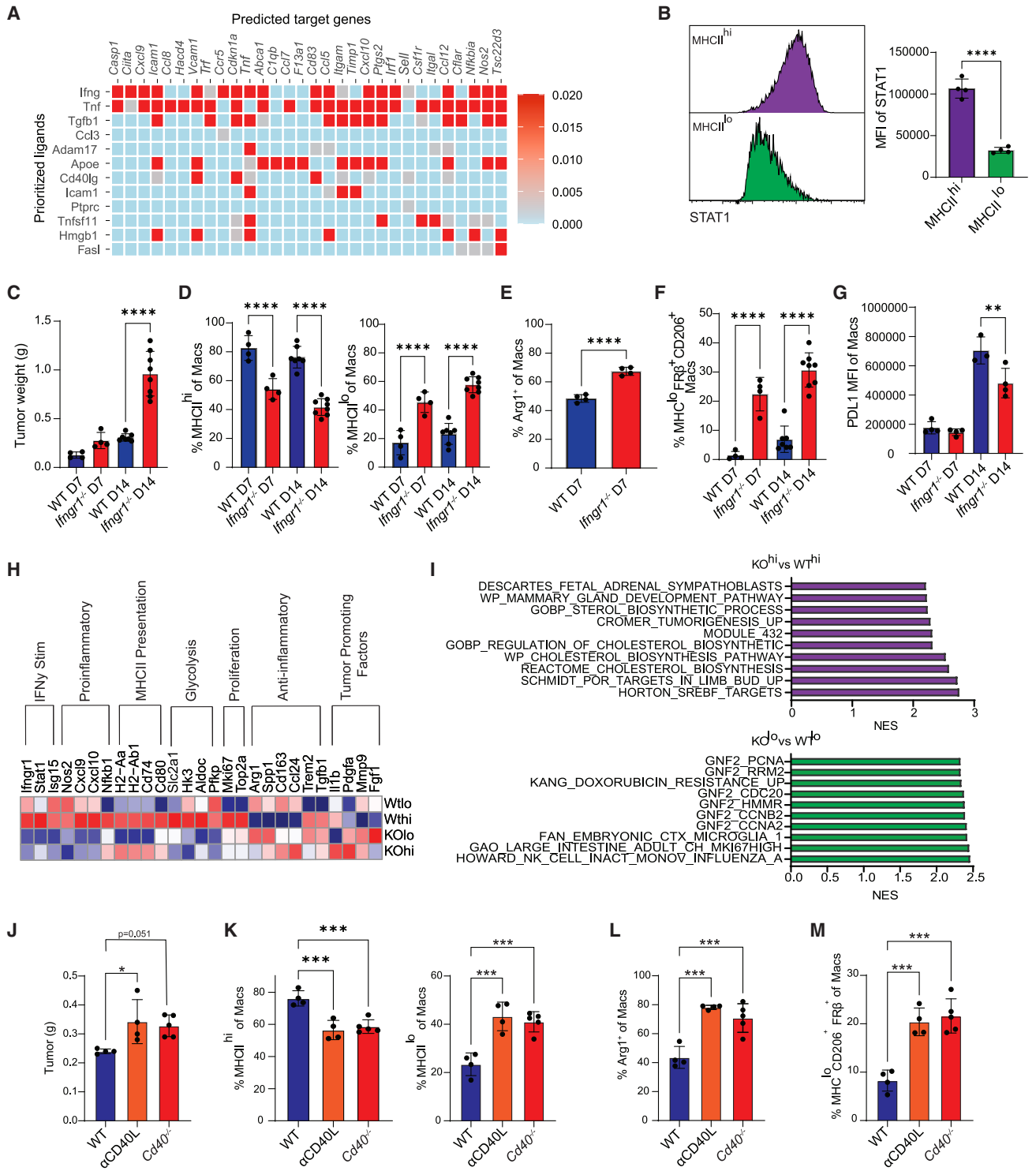

Figure 6. Ifngr1 and CD40 signaling non-redundantly drive anti-tumor TAM fate

(A) NicheNet analysis from scRNA-seq data from Figure 4 using CD4 T cells as donor cells and MHCII^{hi} macrophages as acceptor cells. See also Figure S10.

(B) Stat1 staining and MFI in MHCII^{hi} and MHCII^{lo} intratumoral macrophages at day 7. Data are mean ± SEM; n = 4 mice per group; ****p < 0.0001; Student's t test.

(C) Tumor weights from WT or *Ifngr1*$^{-/-}$ mice; n = 4–8 mice per group; ****p < 0.0001; Student's t test for each time point.

(D) Proportion of MHCII^{hi} or MHCII^{lo} macrophages from WT or *Ifngr1*$^{-/-}$ mice. Data are mean ± SEM; n = 4–8 mice per group; ****p < 0.0001; Student's t test for each time point.

(E) Proportion of Arg1^{+} macrophages on day 7. Data are mean ± SEM; ****p < 0.0001; Student's t test.

(legend continued on next page)

To elucidate transcriptomic changes driven by IFNγR signaling on TAMs, we performed bulk RNA sequencing on sorted MHCII^{hi} and MHCII^{lo} tumor macrophages from WT or *Ifngr1*$^{-/-}$ mice (Figure S11). Differentially expressed gene (DEG) analysis showed a downregulation in IFNγ-stimulated and pro-inflammatory genes in both MHCII^{hi} and MHCII^{lo} populations from *Ifngr1*$^{-/-}$ macrophages, with a compensatory increase in anti-inflammatory genes (Figure 6H). Moreover, *IL1b*, *Pdgfa*, and *Fgf1*, which promote tumor growth,[47–49] were increased in *Ifngr1*$^{-/-}$ macrophages. The MHCII^{hi} population downregulated cell-cycle genes in the absence of IFNγR signaling (Figure 6H), suggesting that, in contrast to a well-established anti-proliferative role, IFNγ can promote MHCII^{hi} macrophage proliferation. Furthermore, there was a decrease in glycolytic genes in *Ifngr1*$^{-/-}$ macrophages, particularly in the MHCII^{hi} population, suggesting that IFNγ promotes MHCII^{hi} macrophage glycolysis. Pathway analysis indicated upregulation of cholesterol metabolism in *Ifngr1*$^{-/-}$ MHCII^{hi} macrophages, consistent with metabolic reprogramming (Figure 6I). Pathway analysis of the MHCII^{lo} subsets revealed an enrichment of processes involved in proliferation in *Ifngr1*$^{-/-}$ macrophages (Figure 6I). Overall, the data suggest that IFNγR signaling is a key regulator of monocyte fate specification and has differential effects on macrophage proliferation and metabolism in a subset-specific manner.

Signaling downstream of CD40 was enriched in fate-mapped, monocyte-derived MHCII^{hi} macrophages (Figure 6A). To determine if endogenous CD40/CD40L between CD4 T cells and macrophages promotes anti-tumor TAMs, we blocked this pathway using either anti-CD40L or *Cd40*$^{-/-}$ mice. Genetic loss of CD40 or CD40L blockade caused an increase in tumor weight (Figure 6J). Abrogating CD40/CD40L resulted in TAM populations mirroring those of CD4 T cell-depleted animals, including a decrease in MHCII^{hi} macrophages, an increase in MHCII^{lo} macrophages (Figure 6K), and an expansion of both Arg1^{+} (Figure 6L) and MHCII^{lo}CD206^{+}FRβ^{+} (Figure 6M) macrophages. Such changes were not due to a decrease in CD4 T cell infiltration, activation, or IFNγ production (Figure S12).

Given the proposed role of TNF-α in driving inflammatory macrophages in other models[50] and NicheNet (Figure 6A), we tested if TNF receptor 1 signaling affected macrophage fate by implanting *KPC*2a tumors into *Tnfr1*$^{-/-}$ mice. Although we observed a minor trend for enrichment of MHCII^{hi} macrophages, this was not significant, and the proportion and number of TAM subpopulations were largely similar at day 7 (Figure S13). Together, IFNγ and CD40 rather than Tnfr1 promote MHCII^{hi} anti-tumor TAMs.

Human PDA TAM profiling

To compare our findings with human PDA, we performed a deep characterization of myeloid cells from publicly available human PDA scRNA-seq data.[51] After data integration of human tumors, 14 distinct cell populations were identified (Figures 7A and S14A). We noted abundant populations of both CD4 and CD8 T cells in human PDA, like in *KPC*2a tumors (Figure 4A). Clustering of myeloid cells generated seven unique clusters (Figure 7B). Cluster 4 expressed genes associated with undifferentiated monocytes (*PLAC8*, *CD115*) and lacked granulocytic genes (*ELANE*, *CXCR2*) (Figure S14B), while clusters 0, 1, 2, 3, 5, and 7 expressed genes of differentiated myeloid cells (*CD68*, *CSFR1*) (Figures 7C and S14B). Cluster 0 expressed genes similar to those of the murine Arg1^{+} population (*SPP1*, *FN1*) (Figure 7C), but lacked *ARG1* expression. Cluster 3 expressed genes associated with antigen presentation (*HLA-DQB2*), paralleling the murine MHCII^{hi} macrophages. Cluster 3 also expressed *CD1C* and *CD1D* (Figure 7C), consistent with a phenotypical relationship to monocyte-derived DCs (MoDCs), which have been well defined in humans.[52] Notably, cluster 3 was also enriched for *CD14* and *CSF1R*, which are well-established markers on cells of monocyte lineage[52] (Figure S14B). Cluster 1 was enriched for *FOLR2* (Figure 7C), resembling tissue-resident macrophages in the *KPC*2a tumors and in human breast cancer.[37] Both clusters 2 and 6 were enriched for *TREM2* (Figure 7D), which may mark monocyte-derived TAMs.[37] Cluster 2 expressed higher transcript levels of complement-associated genes like *C1QB*, while cluster 6 expressed higher levels of *GPNMB* (Figures 7C and 7D), supporting heterogeneity among *TREM2*$^{+}$ TAMs. Next, we performed pseudotime analysis to map monocyte differentiation trajectories. Using monocytes as the origin, this model predicted two endpoint trajectories, either to *FOLR2*$^{+}$ and *TREM2*$^{+}$ TAMs or to MHCII^{hi} MoDCs (Figure 7E). Given that our mouse data suggested that CD4 T cells instruct monocyte differentiation toward a more immunostimulatory phenotype, we next predicted potential interactions between CD4 T cells and MoDCs using NicheNet. This algorithm predicted that TNF and CD40/CD40L signaling was enriched between these two populations (Figure 7F).

To examine the relative contributions of TAM subsets, we performed flow cytometry on samples from resected PDA and

(F) Proportion of MHCII^{lo}CD206^{+}FRβ^{+} macrophages from WT or *Ifngr1*$^{-/-}$ mice. Data are mean ± SEM; n = 4–8 mice per group; ****p < 0.0001; Student's t test for each time point.

(G) PD-L1 MFI gated on total macrophages from WT or *Ifngr1*$^{-/-}$ mice. Data are mean ± SEM; **p < 0.005; Student's t test for each time point.

(H) Normalized expression of selected genes from bulk RNA sequencing from sorted live MHCII^{hi} or MHCII^{lo} tumor macrophages from WT and *Ifngr1*$^{-/-}$ mice at day 14. See also Figure S11.

(I) Gene set enrichment analysis (GSEA) of the top 300 differentially expressed genes from sorted cells in (H).

(J) Orthotopic *KPC*2a tumor weights at day 7 from WT control mice, WT mice treated with CD40L blockade (αCD40L), or *Cd40*$^{-/-}$ mice. *p < 0.05; one way ANOVA with Tukey's post test. See also Figure S12.

(K) Proportion of MHCII^{hi} or MHCII^{lo} macrophages. Each dot is an independent mouse. Data are mean ± SEM; n = 4–5 mice per group; ***p < 0.001; one-way ANOVA with Tukey's posttest.

(L) Proportion of Arg1^{+} macrophages. Each dot is an independent mouse. Data are mean ± SEM; n = 4–5 mice per group; ***p < 0.001; one-way ANOVA with Tukey's posttest.

(M) Proportion of MHCII^{lo}CD206^{+}FRβ^{+} macrophages. Each dot is an independent mouse. Data are mean ± SEM; n = 4–5 mice per group; ***p < 0.001; one-way ANOVA with Tukey's posttest. See also Figure S13.

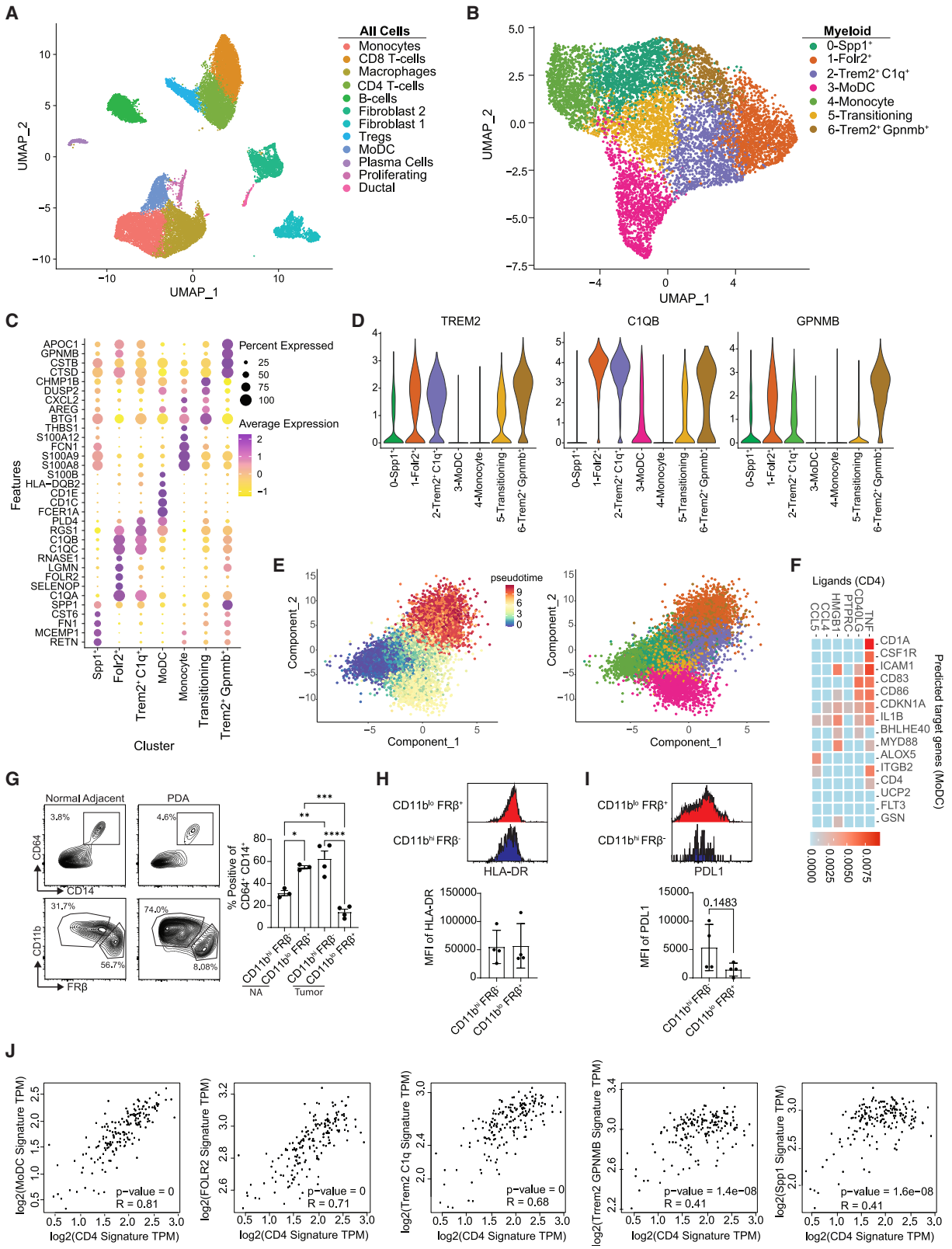

(legend on next page)

normal adjacent human pancreas. We identified two major macrophage populations in normal adjacent tissue and tumor: CD11b^{hi}FRβ^{-} or CD11b^{lo}FRβ^{+} macrophages (Figure 7G). Given that embryonically derived macrophages express lower levels of CD11b,[53] CD11b^{lo}FRβ^{+} may be tissue-resident TAMs. Consistent with this, most macrophages in normal adjacent tissue adopted a CD11b^{lo}FRβ^{+} phenotype; however, within the tumor, more macrophages were CD11b^{hi}FRβ^{-} (Figure 7G), suggesting most of the TAM pool in human PDA is derived from monocytes. Unlike in our mouse model, FRβ^{+} TAMs expressed similar amounts of HLA-DR compared with FRβ^{-} cells (Figure 7H), consistent with FRβ-expressing TAMs in human breast cancer.[37] However, like the *KPC*2a orthotopic PDA model, FRβ^{-} macrophages tended to express higher PD-L1 (Figure 7I), suggesting monocyte-derived CD11b^{hi}FRβ^{-} macrophages may regulate immunity. Finally, to determine if CD4 T cells influence immunostimulatory monocyte differentiation in human PDA, we performed correlation analysis using transcriptomic data of human PDA in GEPIA. Gene signatures for CD4 T cells were derived from our integrated dataset and compared with gene signatures from each macrophage population. CD4 T cell gene signature showed the strongest correlation with MoDCs, while immunosuppressive TREM2^{+} TAMs showed a much weaker correlation (Figure 7J). Thus, while differences in other factors may confound this analysis, the data suggest a link between activated CD4 T cells and MoDC differentiation over immunosuppressive TAM formation.

DISCUSSION

Here, we identify bidirectional crosstalk between macrophages and antigen-specific CD4 T cells that orchestrate anti-tumor immunity in PDA. Our data uncover that tumor-specific CD4 T cells instruct monocyte differentiation into anti-tumor macrophages through cognate antigen recognition and downstream CD40:CD40L and IFNγ pathways. Critically, in the absence of tumor-specific CD4 T cells or MHC class II on monocyte-derived macrophages, monocytes adopt a phenotypic and transcriptomic profile indistinguishable from that of tissue-resident macrophages. Our study uncovers that monocytes can masquerade as tissue-resident TAMs in tumors that lack an MHC class II-restricted tumor antigen, and CD4 T cell recognition of tumor antigen presented by monocyte-derived macrophages may contribute to macrophage heterogeneity in cancer.

Using macrophage fate-mapping approaches in a setting in which tumor-specific T cells are engaged, we show that monocyte and embryonically derived TAMs have distinct phenotypes. We find that most TAMs are derived from monocytes and confirm that embryonically derived TAMs are phenotypically distinct from monocyte-derived TAMs, consistent with a prior study.[24] As tumor-reactive T cells can accelerate monocyte recruitment,[17,27] the contribution of monocytes to the overall TAM pool may be dependent on tumor antigenicity and vary among cancers.

Through direct recognition of tumor cells that express MHC class II, or by effector cytokine production, CD4 T cells can promote tumor rejection in mouse models.[54,55] The adoptive transfer of neoantigen-specific CD4 T cells can lead to solid tumor regressions in advanced cancer patients.[56–58] Here we show that CD4 T cell recognition of tumor antigens presented by monocyte-derived macrophages initiates a cascade of events in the TME that likely work in concert to impede tumor cell growth. Not only did monocytes differentiate into anti-tumor TAMs when they expressed MHC class II, but also overt changes were detected in the T cell compartments, including increasing intratumoral accumulation of Th1 T cells and decreasing Treg and exhausted CD8 T cells. These data highlight that strategies to amplify CD4 T cells that express tumor-specific MHC class II-restricted TCRs are a potent approach for modulating the TME for controlling pancreatic tumor growth.

In other cancer types, CD8 T cell engagement with TAMs has been suggested to promote CD8 T cell exhaustion.[17] In clear cell renal carcinoma, exhausted CD8 T cells and anti-inflammatory macrophages express ligands and receptors that support T cell dysfunction.[16] Here, we show that antigen-specific CD4 T cells promote pro-inflammatory cues within the TME leading to monocyte differentiation into anti-tumor macrophages. CD8 T cells are dispensable for monocyte fate, consistent with the fact that macrophages are not efficient at cross presentation, which is mainly carried out by specific conventional DC subsets *in vivo*.[59] Type I DCs, but not macrophages, are critical for priming and maintaining tumor-specific CD8 T cells in the *KPC*2a model.[26] Type 2 DCs prime naive CD4 T cells in other contexts.[60,61] Thus, monocyte-derived macrophage presentation of tumor antigen locally likely promotes recruitment, proliferation, and/or survival of recently primed CD4 T cells. Reactivation of CD4 T cells by monocyte-derived macrophages may also imprint Th1 lineage commitment.

Figure 7. Profiling of TAMs from human PDA

(A) Uniform manifold approximation and projection (UMAP) of scRNA-seq data from six merged human tumors from Elyada et al.[51] See also Figure S14.

(B) UMAP reclustering of myeloid clusters in (A).

(C) Heatmap of normalized gene expression of the top differentially expressed genes.

(D) Violin plots of selected genes.

(E) Pseudotime of myeloid clusters using Monocle 3 split by pseudotime and by cluster.

(F) NicheNet analysis using CD4 T cells as the donor cluster and MoDCs as the acceptor cluster.

(G) Gating scheme and frequency of myeloid subpopulations from resected human PDA (n = 4) and normal adjacent (n = 3) tissue. Gated on live, CD15^{-} cells. Data are mean ± SEM; *p < 0.05, **p < 0.005, ***p < 0.001, ****p < 0.0001; one-way ANOVA with Tukey's posttest.

(H) Representative HLA-DR staining and HLA-DR MFI from CD11b^{hi}FRβ^{-} and CD11b^{lo}FRβ^{+} macrophages from human PDA and normal adjacent tissue. Data are mean ± SEM. Each dot is an independent sample.

(I) Representative PD-L1 staining and PD-L1 MFI of each population isolated from human PDA.

(J) Correlation of CD4 gene signatures with macrophage subpopulation gene signatures in human PDA. TCGA datasets were determined using GEPIA2. Gene signatures were derived from the top 5 DEGs from (B).

Our data support that tumor-specific CD4 T cell instruction of monocyte fate rather than stochastic cell-intrinsic fate choices underlies macrophage heterogeneity in cancer. Monocytes can differentiate into immunostimulatory monocyte-derived DCs or immunosuppressive TAMs in human PDA,[62] supporting our findings here. CD4-TAM interplay occurs in other models where infusion of tumor-reactive T cells leads to upregulation of inflammatory markers on TAMs[63]; however, it was unclear if this was a repolarization event or changes in tumor-infiltrating monocyte fate decisions. Th2 CD4 T cells can skew macrophages toward an anti-inflammatory state within tumors,[64] highlighting the linkage between macrophages and CD4 T cells. Since macrophages acquire tumor debris within the TME,[26] and fate is governed by antigen-specific CD4 T cells, it is likely that T cell-mediated instruction of macrophage fate is occurring intratumorally.

Resident macrophages appear predisposed to adopt a pro-tumor state and contribute to tumor growth.[24,65–67] Our observations suggest that tissue-resident macrophages are resistant toward rewiring to an immunostimulatory state and that, in the absence of tumor-specific CD4 T cells, monocytes adopt tissue-resident features. Thus, a fate-mapping approach is likely critical for distinguishing monocyte-derived from embryonic-derived TAMs. As embryonically derived macrophages become highly proliferative following CD4 T cell depletion, they may produce factors that direct infiltrating monocyte fate toward a similar tissue-resident-like state.

Human PDA has been stratified into squamous, pancreatic progenitor, immunogenic, or aberrantly differentiated endocrine exocrine genomic subtypes.[18] The immunogenic subset contains genes enriched for T cells and myeloid cells,[18] consistent with our cellular analysis of tumor-infiltrating immune cells in resected human PDA[13] and the *KPC*2a model used herein.[30] While the nature of the neoepitopes in human PDA is unknown, neoantigen quality correlates with long-term survival in PDA,[7,68] human PDA can harbor neoantigen-reactive CD4 T cells,[69] and a personalized neoantigen vaccine containing both MHC class I and MHC class II epitopes can stimulate T cells in human PDA.[70] Together, our findings support a pivotal role for tumor-specific CD4 T cells in governing anti-tumor macrophage fate and inform immunotherapy design by directing efforts to engage anti-tumor CD4 T cells.

Limitations of the study

While Arg1^{+} [39,71] and Lyve1^{+} [67] macrophages are immunosuppressive and promote tumor progression in other cancer models, we did not directly test if deletion of these subsets led to improved outcomes in PDA. While CD40L is reported to be mostly restricted to CD4 T cells[72,73] and CD4 T cells are potent producers of IFNγ,[74,75] we did not test the CD4 T cell intrinsic role of these molecules on macrophage phenotype. Our study is focused on invasive rather than preinvasive disease, and thus our claims apply to understanding advanced disease.

STAR★METHODS

Detailed methods are provided in the online version of this paper and include the following:

SUPPLEMENTAL INFORMATION

Supplemental information can be found online at https://doi.org/10.1016/j.celrep.2023.112732.

ACKNOWLEDGMENTS

We acknowledge the University of Minnesota Flow Cytometry Core and Research Animal Resource facility. M.T.P. is supported by an AHA predoctoral fellowship (903380). Z.C.S. is supported by a NIH T32 AG029796 followed by NIH F31CA275289. M.M.F. was supported by the Ministry of Science and Higher Education of the Russian Federation (agreement 075-15-2022-301). K.Z. was supported by the Priority 2030 Federal Academic Leadership Program. J.W.W. is supported by NIH R01AI165553 and AHA CDA 855022. I.M.S. is supported by NIH R01CA249393, R01CA255039, and P01CA254849; Department of Defense PA200286; a PanCAN-AACR Catalyst Award (19-35-STRO); and an American Cancer Society Institutional Research Grant (124166-IRG-58-001-55-IRG65).

AUTHOR CONTRIBUTIONS

M.T.P., J.W.W., and I.M.S. conceptualized the study and designed experiments. A.L.B. contributed to study design. M.T.P., A.L.B., Y.X., Z.C.S., P.R.S., A.E.K., E.A.M., E.C.-H., G.H.H., and S.B. performed experiments. M.T.P. and Y.X. analyzed data, interpreted data, and prepared figures. Y.X., M.M.F., and K.Z. performed scRNA-seq analyses. M.T.P. and I.M.S. wrote the manuscript. A.L.B. and J.W.W. edited the manuscript.

DECLARATION OF INTERESTS

The authors declare no competing interests.

INCLUSION AND DIVERSITY

We support inclusive, diverse, and equitable conduct of research.

Received: November 11, 2022
Revised: April 21, 2023
Accepted: June 16, 2023
Published: July 3, 2023

REFERENCES

1. Siegel, R.L., Miller, K.D., Fuchs, H.E., and Jemal, A. (2022). Cancer statistics, 2022. Ca - Cancer J. Clin. *72*, 7–33. https://doi.org/10.3322/caac.21708.
2. Schmiechen, Z.C., and Stromnes, I.M. (2020). Mechanisms governing immunotherapy resistance in pancreatic ductal adenocarcinoma. Front. Immunol. *11*, 613815. https://doi.org/10.3389/fimmu.2020.613815.
3. Feig, C., Gopinathan, A., Neesse, A., Chan, D.S., Cook, N., and Tuveson, D.A. (2012). The pancreas cancer microenvironment. Clin. Cancer Res. *18*, 4266–4276. https://doi.org/10.1158/1078-0432.CCR-11-3114.
4. Kiryu, S., Ito, Z., Suka, M., Bito, T., Kan, S., Uchiyama, K., Saruta, M., Hata, T., Takano, Y., Fujioka, S., et al. (2021). Prognostic value of immune factors in the tumor microenvironment of patients with pancreatic ductal adenocarcinoma. BMC Cancer *21*, 1197. https://doi.org/10.1186/s12885-021-08911-4.
5. Ino, Y., Yamazaki-Itoh, R., Shimada, K., Iwasaki, M., Kosuge, T., Kanai, Y., and Hiraoka, N. (2013). Immune cell infiltration as an indicator of the immune microenvironment of pancreatic cancer. Br. J. Cancer *108*, 914–923. https://doi.org/10.1038/bjc.2013.32.
6. Mahajan, U.M., Langhoff, E., Goni, E., Costello, E., Greenhalf, W., Halloran, C., Ormanns, S., Kruger, S., Boeck, S., Ribback, S., et al. (2018). Immune cell and stromal signature associated with progression-free survival of patients with resected pancreatic ductal adenocarcinoma. Gastroenterology *155*, 1625–1639.e2. https://doi.org/10.1053/j.gastro.2018.08.009.
7. Balachandran, V.P., Łuksza, M., Łuksza, M., Makarov, V., Moral, J.A., Remark, R., Herbst, B., Askan, G., Bhanot, U., Senbabaoglu, Y., et al. (2017). Identification of unique neoantigen qualities in long-term survivors of pancreatic cancer. Nature *551*, 512–516. https://doi.org/10.1038/nature24462.
8. Stromnes, I.M., Brockenbrough, J.S., Izeradjene, K., Carlson, M.A., Cuevas, C., Simmons, R.M., Greenberg, P.D., and Hingorani, S.R. (2014). Targeted depletion of an MDSC subset unmasks pancreatic ductal adenocarcinoma to adaptive immunity. Gut *63*, 1769–1781. https://doi.org/10.1136/gutjnl-2013-306271.
9. Stromnes, I.M., DelGiorno, K.E., Greenberg, P.D., and Hingorani, S.R. (2014). Stromal reengineering to treat pancreas cancer. Carcinogenesis *35*, 1451–1460. https://doi.org/10.1093/carcin/bgu115.
10. Bayne, L.J., Beatty, G.L., Jhala, N., Clark, C.E., Rhim, A.D., Stanger, B.Z., and Vonderheide, R.H. (2012). Tumor-derived granulocyte-macrophage colony-stimulating factor regulates myeloid inflammation and T cell immunity in pancreatic cancer. Cancer Cell *21*, 822–835. https://doi.org/10.1016/j.ccr.2012.04.025.
11. Pylayeva-Gupta, Y., Lee, K.E., Hajdu, C.H., Miller, G., and Bar-Sagi, D. (2012). Oncogenic Kras-induced GM-CSF production promotes the development of pancreatic neoplasia. Cancer Cell *21*, 836–847. https://doi.org/10.1016/j.ccr.2012.04.024.
12. Clark, C.E., Hingorani, S.R., Mick, R., Combs, C., Tuveson, D.A., and Vonderheide, R.H. (2007). Dynamics of the immune reaction to pancreatic cancer from inception to invasion. Cancer Res. *67*, 9518–9527. https://doi.org/10.1158/0008-5472.CAN-07-0175.
13. Stromnes, I.M., Hulbert, A., Pierce, R.H., Greenberg, P.D., and Hingorani, S.R. (2017). T-Cell localization, activation, and clonal expansion in human pancreatic ductal adenocarcinoma. Cancer Immunol. Res. *5*, 978–991. https://doi.org/10.1158/2326-6066.CIR-16-0322.
14. Halbrook, C.J., Pontious, C., Kovalenko, I., Lapienyte, L., Dreyer, S., Lee, H.-J., Thurston, G., Zhang, Y., Lazarus, J., Sajjakulnukit, P., et al. (2019). Macrophage-released pyrimidines inhibit gemcitabine therapy in pancreatic cancer. Cell Metabol. *29*, 1390–1399.e6. https://doi.org/10.1016/j.cmet.2019.02.001.
15. Mitchem, J.B., Brennan, D.J., Knolhoff, B.L., Belt, B.A., Zhu, Y., Sanford, D.E., Belaygorod, L., Carpenter, D., Collins, L., Piwnica-Worms, D., et al. (2013). Targeting tumor-infiltrating macrophages decreases tumor-initiating cells, relieves immunosuppression, and improves chemotherapeutic responses. Cancer Res. *73*, 1128–1141. https://doi.org/10.1158/0008-5472.CAN-12-2731.
16. Braun, D.A., Street, K., Burke, K.P., Cookmeyer, D.L., Denize, T., Pedersen, C.B., Gohil, S.H., Schindler, N., Pomerance, L., Hirsch, L., et al. (2021). Progressive immune dysfunction with advancing disease stage in renal cell carcinoma. Cancer Cell *39*, 632–648.e8. https://doi.org/10.1016/j.ccell.2021.02.013.
17. Kersten, K., Hu, K.H., Combes, A.J., Samad, B., Harwin, T., Ray, A., Rao, A.A., Cai, E., Marchuk, K., Artichoker, J., et al. (2022). Spatiotemporal co-dependency between macrophages and exhausted CD8+ T cells in cancer. Cancer Cell *40*, 624–638.e9. https://doi.org/10.1016/j.ccell.2022.05.004.
18. Bailey, P., Chang, D.K., Nones, K., Johns, A.L., Patch, A.M., Gingras, M.C., Miller, D.K., Christ, A.N., Bruxner, T.J.C., Quinn, M.C., et al. (2016). Genomic analyses identify molecular subtypes of pancreatic cancer. Nature *531*, 47–52. https://doi.org/10.1038/nature16965.
19. Ma, R.-Y., Black, A., and Qian, B.-Z. (2022). Macrophage diversity in cancer revisited in the era of single-cell omics. Trends Immunol. *43*, 546–563. https://doi.org/10.1016/j.it.2022.04.008.
20. Chijimatsu, R., Kobayashi, S., Takeda, Y., Kitakaze, M., Tatekawa, S., Arao, Y., Nakayama, M., Tachibana, N., Saito, T., Ennishi, D., et al. (2022). Establishment of a reference single-cell RNA sequencing dataset for human pancreatic adenocarcinoma. iScience *25*, 104659. https://doi.org/10.1016/j.isci.2022.104659.
21. Christofides, A., Strauss, L., Yeo, A., Cao, C., Charest, A., and Boussiotis, V.A. (2022). The complex role of tumor-infiltrating macrophages. Nat. Immunol. *23*, 1148–1156. https://doi.org/10.1038/s41590-022-01267-2.
22. Casanova-Acebes, M., Dalla, E., Leader, A.M., LeBerichel, J., Nikolic, J., Morales, B.M., Brown, M., Chang, C., Troncoso, L., Chen, S.T., et al. (2021). Tissue-resident macrophages provide a pro-tumorigenic niche to early NSCLC cells. Nature *595*, 578–584. https://doi.org/10.1038/s41586-021-03651-8.
23. Franklin, R.A., and Li, M.O. (2016). Ontogeny of tumor-associated macrophages and its implication in cancer regulation. Trends Cancer *2*, 20–34. https://doi.org/10.1016/j.trecan.2015.11.004.
24. Zhu, Y., Herndon, J.M., Sojka, D.K., Kim, K.-W., Knolhoff, B.L., Zuo, C., Cullinan, D.R., Luo, J., Bearden, A.R., Lavine, K.J., et al. (2017). Tissue-resident macrophages in pancreatic ductal adenocarcinoma originate from embryonic hematopoiesis and promote tumor progression. Immunity *47*, 323–338.e6. https://doi.org/10.1016/j.immuni.2017.07.014.
25. Zhu, Y., Knolhoff, B.L., Meyer, M.A., Nywening, T.M., West, B.L., Luo, J., Wang-Gillam, A., Goedegebuure, S.P., Linehan, D.C., and DeNardo, D.G. (2014). CSF1/CSF1R blockade reprograms tumor-infiltrating macrophages and improves response to T-cell checkpoint immunotherapy in pancreatic cancer models. Cancer Res. *74*, 5057–5069. https://doi.org/10.1158/0008-5472.CAN-13-3723.
26. Burrack, A.L., Schmiechen, Z.C., Patterson, M.T., Miller, E.A., Spartz, E.J., Rollins, M.R., Raynor, J.F., Mitchell, J.S., Kaisho, T., Fife, B.T., and Stromnes, I.M. (2022). Distinct myeloid antigen-presenting cells dictate differential fates of tumor-specific CD8+ T cells in pancreatic cancer. JCI Insight *7*, e151593. https://doi.org/10.1172/jci.insight.151593.
27. Stromnes, I.M., Burrack, A.L., Hulbert, A., Bonson, P., Black, C., Brockenbrough, J.S., Raynor, J.F., Spartz, E.J., Pierce, R.H., Greenberg, P.D., and Hingorani, S.R. (2019). Differential effects of depleting versus programming tumor-associated macrophages on engineered T cells in pancreatic ductal adenocarcinoma. Cancer Immunol. Res. *7*, 977–989. https://doi.org/10.1158/2326-6066.CIR-18-0448.
28. Ho, W.J., and Jaffee, E.M. (2021). Macrophage-targeting by CSF1/1R blockade in pancreatic cancers. Cancer Res. *81*, 6071–6073. https://doi.org/10.1158/0008-5472.CAN-21-3603.
29. Byrne, K.T., and Vonderheide, R.H. (2016). CD40 stimulation obviates innate sensors and drives T cell immunity in cancer. Cell Rep. *15*, 2719–2732. https://doi.org/10.1016/j.celrep.2016.05.058.

30. Burrack, A.L., Spartz, E.J., Raynor, J.F., Wang, I., Olson, M., and Stromnes, I.M. (2019). Combination PD-1 and PD-L1 blockade promotes durable neoantigen-specific T cell-mediated immunity in pancreatic ductal adenocarcinoma. Cell Rep. *28*, 2140–2155.e6. https://doi.org/10.1016/j.celrep.2019.07.059.

31. Xu, Y., Schrank, P.R., and Williams, J.W. (2022). Macrophage fate mapping. Curr. Protoc. *2*, e456. https://doi.org/10.1002/cpz1.456.

32. Dolfi, B., Gallerand, A., Firulyova, M.M., Xu, Y., Merlin, J., Dumont, A., Castiglione, A., Vaillant, N., Quemener, S., Gerke, H., et al. (2022). Unravelling the sex-specific diversity and functions of adrenal gland macrophages. Cell Rep. *39*, 110949. https://doi.org/10.1016/j.celrep.2022.110949.

33. Gallerand, A., Stunault, M.I., Merlin, J., Luehmann, H.P., Sultan, D.H., Firulyova, M.M., Magnone, V., Khedher, N., Jalil, A., Dolfi, B., et al. (2021). Brown adipose tissue monocytes support tissue expansion. Nat. Commun. *12*, 5255. https://doi.org/10.1038/s41467-021-25616-1.

34. Calderon, B., Carrero, J.A., Ferris, S.T., Sojka, D.K., Moore, L., Epelman, S., Murphy, K.M., Yokoyama, W.M., Randolph, G.J., and Unanue, E.R. (2015). The pancreas anatomy conditions the origin and properties of resident macrophages. J. Exp. Med. *212*, 1497–1512. https://doi.org/10.1084/jem.20150496.

35. Yona, S., Kim, K.-W., Wolf, Y., Mildner, A., Varol, D., Breker, M., Strauss-Ayali, D., Viukov, S., Guilliams, M., Misharin, A., et al. (2013). Fate mapping reveals origins and dynamics of monocytes and tissue macrophages under homeostasis. Immunity *38*, 79–91. https://doi.org/10.1016/j.immuni.2012.12.001.

36. Srinivasan, A., Foley, J., Ravindran, R., and McSorley, S.J. (2004). Low-dose Salmonella infection evades activation of flagellin-specific CD4 T cells. J. Immunol. *173*, 4091–4099. https://doi.org/10.4049/jimmunol.173.6.4091.

37. Nalio Ramos, R., Missolo-Koussou, Y., Gerber-Ferder, Y., Bromley, C.P., Bugatti, M., Núñez, N.G., Tosello Boari, J., Richer, W., Menger, L., Denizeau, J., et al. (2022). Tissue-resident FOLR2+ macrophages associate with CD8+ T cell infiltration in human breast cancer. Cell *185*, 1189–1207.e25. https://doi.org/10.1016/j.cell.2022.02.021.

38. Dawson, C.A., Pal, B., Vaillant, F., Gandolfo, L.C., Liu, Z., Bleriot, C., Ginhoux, F., Smyth, G.K., Lindeman, G.J., Mueller, S.N., et al. (2020). Tissue-resident ductal macrophages survey the mammary epithelium and facilitate tissue remodelling. Nat. Cell Biol. *22*, 546–558. https://doi.org/10.1038/s41556-020-0505-0.

39. Arlauckas, S.P., Garren, S.B., Garris, C.S., Kohler, R.H., Oh, J., Pittet, M.J., and Weissleder, R. (2018). Arg1 expression defines immunosuppressive subsets of tumor-associated macrophages. Theranostics *8*, 5842–5854. https://doi.org/10.7150/thno.26888.

40. Cheng, S., Li, Z., Gao, R., Xing, B., Gao, Y., Yang, Y., Qin, S., Zhang, L., Ouyang, H., Du, P., et al. (2021). A pan-cancer single-cell transcriptional atlas of tumor infiltrating myeloid cells. Cell *184*, 792–809.e23. https://doi.org/10.1016/j.cell.2021.01.010.

41. Trapnell, C., Cacchiarelli, D., Grimsby, J., Pokharel, P., Li, S., Morse, M., Lennon, N.J., Livak, K.J., Mikkelsen, T.S., and Rinn, J.L. (2014). The dynamics and regulators of cell fate decisions are revealed by pseudotemporal ordering of single cells. Nat. Biotechnol. *32*, 381–386. https://doi.org/10.1038/nbt.2859.

42. Browaeys, R., Saelens, W., and Saeys, Y. (2020). NicheNet: modeling intercellular communication by linking ligands to target genes. Nat. Methods *17*, 159–162. https://doi.org/10.1038/s41592-019-0667-5.

43. Burrack, A.L., Rollins, M.R., Spartz, E.J., Mesojednik, T.D., Schmiechen, Z.C., Raynor, J.F., Wang, I.X., Kedl, R.M., and Stromnes, I.M. (2021). CD40 agonist overcomes T cell exhaustion induced by chronic myeloid cell IL-27 production in a pancreatic cancer preclinical model. J. Immunol. *206*, 1372–1384. https://doi.org/10.4049/jimmunol.2000765.

44. Carlin, A.F., Vizcarra, E.A., Branche, E., Viramontes, K.M., Suarez-Amaran, L., Ley, K., Heinz, S., Benner, C., Shresta, S., and Glass, C.K. (2018). Deconvolution of pro- and antiviral genomic responses in Zika virus-infected and bystander macrophages. Proc. Natl. Acad. Sci. USA *115*, E9172–E9181. https://doi.org/10.1073/pnas.1807690115.

45. Mimura, K., Teh, J.L., Okayama, H., Shiraishi, K., Kua, L.-F., Koh, V., Smoot, D.T., Ashktorab, H., Oike, T., Suzuki, Y., et al. (2018). PD-L1 expression is mainly regulated by interferon gamma associated with JAK-STAT pathway in gastric cancer. Cancer Sci. *109*, 43–53. https://doi.org/10.1111/cas.13424.

46. Garcia-Diaz, A., Shin, D.S., Moreno, B.H., Saco, J., Escuin-Ordinas, H., Rodriguez, G.A., Zaretsky, J.M., Sun, L., Hugo, W., Wang, X., et al. (2017). Interferon receptor signaling pathways regulating PD-L1 and PD-L2 expression. Cell Rep. *19*, 1189–1201. https://doi.org/10.1016/j.celrep.2017.04.031.

47. Das, S., Shapiro, B., Vucic, E.A., Vogt, S., and Bar-Sagi, D. (2020). Tumor cell-derived IL1β promotes desmoplasia and immune suppression in pancreatic cancer. Cancer Res. *80*, 1088–1101. https://doi.org/10.1158/0008-5472.CAN-19-2080.

48. Sahraei, M., Roy, L.D., Curry, J.M., Teresa, T.L., Nath, S., Besmer, D., Kidiyoor, A., Dalia, R., Gendler, S.J., and Mukherjee, P. (2012). MUC1 regulates PDGFA expression during pancreatic cancer progression. Oncogene *31*, 4935–4945. https://doi.org/10.1038/onc.2011.651.

49. Bhattacharyya, S., Oon, C., Kothari, A., Horton, W., Link, J., Sears, R.C., and Sherman, M.H. (2020). Acidic fibroblast growth factor underlies microenvironmental regulation of MYC in pancreatic cancer. J. Exp. Med. *217*, e20191805. https://doi.org/10.1084/jem.20191805.

50. Mysore, V., Tahir, S., Furuhashi, K., Arora, J., Rosetti, F., Cullere, X., Yazbeck, P., Sekulic, M., Lemieux, M.E., Raychaudhuri, S., et al. (2022). Monocytes transition to macrophages within the inflamed vasculature via monocyte CCR2 and endothelial TNFR2. J. Exp. Med. *219*, e20210562. https://doi.org/10.1084/jem.20210562.

51. Elyada, E., Bolisetty, M., Laise, P., Flynn, W.F., Courtois, E.T., Burkhart, R.A., Teinor, J.A., Belleau, P., Biffi, G., Lucito, M.S., et al. (2019). Cross-species single-cell analysis of pancreatic ductal adenocarcinoma reveals antigen-presenting cancer-associated fibroblasts. Cancer Discov. *9*, 1102–1123. https://doi.org/10.1158/2159-8290.CD-19-0094.

52. Heger, L., Hofer, T.P., Bigley, V., de Vries, I.J.M., Dalod, M., Dudziak, D., and Ziegler-Heitbrock, L. (2020). Subsets of CD1c+ DCs: dendritic cell versus monocyte lineage. Front. Immunol. *11*, 559166. https://doi.org/10.3389/fimmu.2020.559166.

53. Schulz, C., Gomez Perdiguero, E., Chorro, L., Szabo-Rogers, H., Cagnard, N., Kierdorf, K., Prinz, M., Wu, B., Jacobsen, S.E.W., Pollard, J.W., et al. (2012). A lineage of myeloid cells independent of Myb and hematopoietic stem cells. Science *336*, 86–90. https://doi.org/10.1126/science.1219179.

54. Poncette, L., Bluhm, J., and Blankenstein, T. (2022). The role of CD4 T cells in rejection of solid tumors. Curr. Opin. Immunol. *74*, 18–24. https://doi.org/10.1016/j.coi.2021.09.005.

55. Alspach, E., Lussier, D.M., Miceli, A.P., Kizhvatov, I., DuPage, M., Luoma, A.M., Meng, W., Lichti, C.F., Esaulova, E., Vomund, A.N., et al. (2019). MHC-II neoantigens shape tumour immunity and response to immunotherapy. Nature *574*, 696–701. https://doi.org/10.1038/s41586-019-1671-8.

56. Tran, E., Turcotte, S., Gros, A., Robbins, P.F., Lu, Y.-C., Dudley, M.E., Wunderlich, J.R., Somerville, R.P., Hogan, K., Hinrichs, C.S., et al. (2014). Cancer immunotherapy based on mutation-specific CD4+ T cells in a patient with epithelial cancer. Science *344*, 641–645. https://doi.org/10.1126/science.1251102.

57. Linnemann, C., van Buuren, M.M., Bies, L., Verdegaal, E.M.E., Schotte, R., Calis, J.J.A., Behjati, S., Velds, A., Hilkmann, H., Atmioui, D.E., et al. (2015). High-throughput epitope discovery reveals frequent recognition of neo-antigens by CD4+ T cells in human melanoma. Nat. Med. *21*, 81–85. https://doi.org/10.1038/nm.3773.

58. Veatch, J.R., Lee, S.M., Fitzgibbon, M., Chow, I.-T., Jesernig, B., Schmitt, T., Kong, Y.Y., Kargl, J., Houghton, A.M., Thompson, J.A., et al. (2018). Tumor-infiltrating BRAFV600E-specific CD4+ T cells correlated with

complete clinical response in melanoma. J. Clin. Invest. *128*, 1563–1568. https://doi.org/10.1172/JCI98689.

59. Joffre, O.P., Segura, E., Savina, A., and Amigorena, S. (2012). Cross-presentation by dendritic cells. Nat. Rev. Immunol. *12*, 557–569. https://doi.org/10.1038/nri3254.
60. Binnewies, M., Mujal, A.M., Pollack, J.L., Combes, A.J., Hardison, E.A., Barry, K.C., Tsui, J., Ruhland, M.K., Kersten, K., Abushawish, M.A., et al. (2019). Unleashing type-2 dendritic cells to drive protective antitumor CD4+ T cell immunity. Cell *177*, 556–571.e16. https://doi.org/10.1016/j.cell.2019.02.005.
61. Dudziak, D., Kamphorst, A.O., Heidkamp, G.F., Buchholz, V.R., Trumpfheller, C., Yamazaki, S., Cheong, C., Liu, K., Lee, H.-W., Park, C.G., et al. (2007). Differential antigen processing by dendritic cell subsets in vivo. Science *315*, 107–111. https://doi.org/10.1126/science.1136080.
62. Rodriguez, E., Boelaars, K., Brown, K., Eveline Li, R.J., Kruijssen, L., Bruijns, S.C.M., van Ee, T., Schetters, S.T.T., Crommentuijn, M.H.W., van der Horst, J.C., et al. (2021). Sialic acids in pancreatic cancer cells drive tumour-associated macrophage differentiation via the Siglec receptors Siglec-7 and Siglec-9. Nat. Commun. *12*, 1270. https://doi.org/10.1038/s41467-021-21550-4.
63. Perez-Diez, A., Liu, X., and Matzinger, P. (2022). Neoantigen presentation and IFNγ signaling on the same tumor-associated macrophage are necessary for CD4 T cell-mediated antitumor activity in mice. Cancer Res. Commun. *2*, 316–329. https://doi.org/10.1158/2767-9764.crc-22-0052.
64. DeNardo, D.G., Barreto, J.B., Andreu, P., Vasquez, L., Tawfik, D., Kolhatkar, N., and Coussens, L.M. (2009). CD4(+) T cells regulate pulmonary metastasis of mammary carcinomas by enhancing protumor properties of macrophages. Cancer Cell *16*, 91–102. https://doi.org/10.1016/j.ccr.2009.06.018.
65. Loyher, P.-L., Hamon, P., Laviron, M., Meghraoui-Kheddar, A., Goncalves, E., Deng, Z., Torstensson, S., Bercovici, N., Baudesson de Chanville, C., Combadière, B., et al. (2018). Macrophages of distinct origins contribute to tumor development in the lung. J. Exp. Med. *215*, 2536–2553. https://doi.org/10.1084/jem.20180534.
66. Etzerodt, A., Moulin, M., Doktor, T.K., Delfini, M., Mossadegh-Keller, N., Bajenoff, M., Sieweke, M.H., Moestrup, S.K., Auphan-Anezin, N., and Lawrence, T. (2020). Tissue-resident macrophages in omentum promote metastatic spread of ovarian cancer. J. Exp. Med. *217*, e20191869. https://doi.org/10.1084/jem.20191869.
67. Baer, J.M., Zuo, C., Kang, L.-I., Alarcon de la Lastra, A., Borcherding, N.C., Knolhoff, B.L., Bogner, S.J., Zhu, Y., Lewis, M.A., Zhang, N., et al. (2022). Pancreas resident macrophage-induced fibrosis has divergent roles in pancreas inflammatory injury and PDAC. Preprint at bioRxiv. https://doi.org/10.1101/2022.02.09.479745.
68. Łuksza, M., Sethna, Z.M., Rojas, L.A., Lihm, J., Bravi, B., Elhanati, Y., Soares, K., Amisaki, M., Dobrin, A., Hoyos, D., et al. (2022). Neoantigen quality predicts immunoediting in survivors of pancreatic cancer. Nature *606*, 389–395. https://doi.org/10.1038/s41586-022-04735-9.
69. Meng, Q., Valentini, D., Rao, M., Moro, C.F., Paraschoudi, G., Jäger, E., Dodoo, E., Rangelova, E., del Chiaro, M., and Maeurer, M. (2019). Neoepitope targets of tumour-infiltrating lymphocytes from patients with pancreatic cancer. Br. J. Cancer *120*, 97–108. https://doi.org/10.1038/s41416-018-0262-z.
70. Rojas, L.A., Sethna, Z., Soares, K.C., Olcese, C., Pang, N., Patterson, E., Lihm, J., Ceglia, N., Guasp, P., Chu, A., et al. (2023). Personalized RNA neoantigen vaccines stimulate T cells in pancreatic cancer. Nature *618*, 144–150. https://doi.org/10.1038/s41586-023-06063-y.
71. Fu, Y., Pajulas, A., Wang, J., Zhou, B., Cannon, A., Cheung, C.C.L., Zhang, J., Zhou, H., Fisher, A.J., Omstead, D.T., et al. (2022). Mouse pulmonary interstitial macrophages mediate the pro-tumorigenic effects of IL-9. Nat. Commun. *13*, 3811. https://doi.org/10.1038/s41467-022-31596-7.
72. Grewal, I.S., Xu, J., and Flavell, R.A. (1995). Impairment of antigen-specific T-cell priming in mice lacking CD40 ligand. Nature *378*, 617–620. https://doi.org/10.1038/378617a0.
73. Elgueta, R., Benson, M.J., De Vries, V.C., Wasiuk, A., Guo, Y., and Noelle, R.J. (2009). Molecular mechanism and function of CD40/CD40L engagement in the immune system. Immunol. Rev. *229*, 152–172. https://doi.org/10.1111/j.1600-065X.2009.00782.x.
74. Ngai, P., McCormick, S., Small, C., Zhang, X., Zganiacz, A., Aoki, N., and Xing, Z. (2007). Gamma interferon responses of CD4 and CD8 T-cell subsets are quantitatively different and independent of each other during pulmonary *Mycobacterium bovis* BCG infection. Infect. Immun. *75*, 2244–2252. https://doi.org/10.1128/IAI.00024-07.
75. Green, A.M., DiFazio, R., and Flynn, J.L. (2013). IFN-Γ from CD4 T cells is essential for host survival and enhances CD8 T cell function during *Mycobacterium tuberculosis* infection. J. Immunol. *190*, 270–277. https://doi.org/10.4049/jimmunol.1200061.
76. Croxford, A.L., Lanzinger, M., Hartmann, F.J., Schreiner, B., Mair, F., Pelczar, P., Clausen, B.E., Jung, S., Greter, M., and Becher, B. (2015). The cytokine GM-CSF drives the inflammatory signature of CCR2+ monocytes and licenses autoimmunity. Immunity *43*, 502–514. https://doi.org/10.1016/j.immuni.2015.08.010.
77. Reiley, W.W., Shafiani, S., Wittmer, S.T., Tucker-Heard, G., Moon, J.J., Jenkins, M.K., Urdahl, K.B., Winslow, G.M., and Woodland, D.L. (2010). Distinct functions of antigen-specific CD4 T cells during murine Mycobacterium tuberculosis infection. Proc. Natl. Acad. Sci. USA *107*, 19408–19413. https://doi.org/10.1073/pnas.1006298107.
78. McGinnis, C.S., Murrow, L.M., and Gartner, Z.J. (2019). DoubletFinder: doublet detection in single-cell RNA sequencing data using artificial nearest neighbors. Cell Syst. *8*, 329–337.e4. https://doi.org/10.1016/j.cels.2019.03.003.
79. Korsunsky, I., Millard, N., Fan, J., Slowikowski, K., Zhang, F., Wei, K., Baglaenko, Y., Brenner, M., Loh, P.-R., and Raychaudhuri, S. (2019). Fast, sensitive and accurate integration of single-cell data with Harmony. Nat. Methods *16*, 1289–1296. https://doi.org/10.1038/s41592-019-0619-0.
80. Aran, D., Looney, A.P., Liu, L., Wu, E., Fong, V., Hsu, A., Chak, S., Naikawadi, R.P., Wolters, P.J., Abate, A.R., et al. (2019). Reference-based analysis of lung single-cell sequencing reveals a transitional profibrotic macrophage. Nat. Immunol. *20*, 163–172. https://doi.org/10.1038/s41590-018-0276-y.

STAR★METHODS

KEY RESOURCES TABLE

REAGENT or RESOURCE	SOURCE	IDENTIFIER
Antibodies		
anti-mouse CD45 (clone 30-F11)	BD Bioscience	Cat#: 566168; RRID: AB_2739565
anti-mouse Ly6C (clone HK1.4)	Biolegend	Cat#: 128031; AB_2562177
anti-mouse CD11b (clone M1/70)	Biolegend	Cat#: 101237; RRID: AB_11126744
anti-mouse F4/80 (clone BM8)	Biolegend	Cat#: 123149; RRID: AB_2564589
anti-mouse Ly6G (clone 1A8)	Biolegend	Cat#: 127645; RRID: AB_2566317
anti-mouse CD206 (clone C068C2)	Biolegend	Cat#: 141715; AB_2561991
anti-mouse PD-L1 (clone 10F.9G2)	Biolegend	Cat#: 124313; RRID: AB_10639934
anti-mouse FRβ (clone 10F.9G2)	Biolegend	Cat#: 153305; RRID: AB_2721312
anti-mouse Arg1 (clone A1exF5)	ThermoFisher	Cat#: 25369782: RRID: AB_2734841
anti-mouse I-A/I-E (clone M5/114.15.2)	Biolegend	Cat#: 107651; RRID: AB_2616728
anti-mouse Ki67 (clone 16A6)	Biolegend	Cat#: 652420; RRID: AB_2564285
anti-mouse CD3 (clone 17A2)	BD Bioscience	Cat#: 740530: RRID:AB_2740239
anti-mouse CD8 (clone 53-6.7)	Biolegend	Cat#: 100759; RRID: AB_2563510
anti-mouse CD44 (clone IM7)	Tonbo Bioscience	Cat#: 65-0041; RRID:AB_2621847
anti-mouse CD4 (clone RM4-5)	ThermoFisher	Cat#: 56004282; RRID: AB_494000
anti-mouse Klrg1 (clone 2F1)	eBioscience	Cat#: 25589382; RRID: AB_1518768
anti-mouse Foxp3 (clone FJK-16s)	eBioscience	Cat#: 48577382; RRID: AB_1518812
anti-mouse T-bet (clone 4B10)	Biolegend	Cat#: 644810; RRID: AB_2200542
anti-mouse Stat1 (clone D1K9Y)	Cell Signaling	Cat#: 80916S
anti-mouse IFNγ (clone XMG1.2)	Invitrogen	Cat#: 24731141
anti-mouse CD19 (clone 1D3)	Biolegend	Cat#: 152403; RRID: AB_2629812
anti-mouse CD115 (clone AFS98)	Biolegend	Cat#:135525: RRID: AB_2566461
anti-mouse Lyve1 (clone ALY7)	ThermoFisher	Cat#: 14-0443-82
anti-human CD11b (clone ICRF44)	Biolegend	Cat#: 301310; RRID:AB_314162
anti-human CD11c (clone 3.9)	eBioscience	Cat#: 25016642
anti-human CD64 (clone 10.1)	Biolegend	Cat#: 305036; RRID: AB_2650834
anti-human CD14 (clone 61D3)	ThermoFisher	Cat#: 11014942; RRID:AB_10597597
anti-human CD15 (clone HI98)	BD Bioscience	Cat#: 564232; RRID: AB_2738686
anti-human FRβ (clone 94b)	Biolegend	Cat#: 391703; RRID: AB_2721335
anti-human HLA-DR (clone L243)	BD Bioscience	Cat#: 552764; RRID: AB_394453
anti-human PD-L1 (clone 29E.2A3)	Biolegend	Cat#: 329722; RRID: AB_2565764
anti-human CD163 (clone GHI/61)	Biolegend	Cat#: 333632; RRID: AB_2728288
InVivoMAb anti-mouse CD4 (clone GK1.5)	BioXcell	Cat#:BE0003-1; RRID: AB_1107636
InVivoMAb anti-mouse CD8 (clone 2.43)	BioXcell	Cat#:BE0061; RRID: AB_1125541
InVivoMAb anti-mouse CD40L (clone MR1)	BioXcell	Cat#:BE0017-1; RRID: AB_1107601
TotalSeq™-A0190 anti-mouse CD274	Biolegend	Cat#:153604; RRID: AB_2783125
TotalSeq™-A0564 anti-mouse FRβ	Biolegend	Cat#:153307; RRID: AB_2800690
TotalSeq™-A0117 anti-mouse I-A/I-E	Biolegend	Cat#: 107653; RRID: AB_2750505
Biological samples		
Patient PDA Samples	University of Minnesota BioNet	N/A
Chemicals, peptides, and recombinant proteins		
PFA 4%	VWR International	Cat#: 9713.1000
Tamoxifen	Sigma	Cat#: T5648

(*Continued on next page*)

Continued

REAGENT or RESOURCE	SOURCE	IDENTIFIER
DMEM medium	Life Technologies	Cat#: 21875091
Red blood cell lysis buffer	BD Bioscience	Cat#: 555899
Fetal bovine serum	ThermoFisher	Cat#: 12350273
Amphotericin B	GIBCO	Cat#: 15290018
Penicillin/streptomycin	GIBCO	Cat#: 10378016
Dextrose	ThermoFisher	Cat#: D15-500
EDTA	ThermoFisher	Cat#: 15575020
L-Glutamate	ThermoFisher	Cat#: 25030081
β-mercaptoethanol	GIBCO	Cat#: M6250
Ghost viability dye BV540	Tonbo	Cat#: 13-0879-T100
Golgiplug	BD Bioscience	Cat#: 555029
Collagenase IV	Sigma Aldrich	Cat#: V900893
Critical commercial assays		
Foxp3 fixation and permeabilization kit	Tonbo	Cat#: TNB-0607-KIT
CD4+ T Cell Isolation Kit, mouse	Miltenyi	Cat # 130-092-916
Cell Stimulation Cocktail (500X)	eBioscience	Cat#: 00-4970-03
Deposited data		
Mouse scRNAseq	GEO	GSE233068
Mouse Bulkseq	GEO	GSE233068
Experimental models: Cell lines		
KPC2a cells	Burrack *et. al.*[30]	N/A
KPC OVA cells	Burrack *et. al.*[30]	N/A
Experimental models: Organisms/strains		
C57BL/6J mice	Jackson Labs	000664
Ifngr1-/-	Jackson Labs	003288
Tnfrsf1a-/-	Jackson Labs	003242
Cd40-/-	Jackson Labs	002928
CX3CR1^{CreER} (B6.129P2(C)-Cx3cr1tm2.1 (cre/ERT2)Jung/J)	Jackson Labs	020940
CCR2^{creERT2} [C57BL/6NTac-Ccr2tm2982 (T2A-Cre7ESR1-T2A-mKate2)]	Croxford *et. al.*[76]	N/A
R26-tdTomato (B6.Cg-Gt(ROSA)26Sortm9 (CAG-tdTomato)Hze/J).	Jackson Labs	007909
CCR2-CreER-GFP (C57BL/6-Ccr2em1 (icre/ERT2)Peng/J) x I-AB-flox (B6.129X1-H2-Ab1tm1Koni/J)	This report	N/A
Sm1xRag1-/-	Srinivasan *et. al.*[36]	N/A
Rag1-/- (B6.Cg-Rag2tm1.1Cgn/J)	Jackson Labs	008309
OTII (B6.Cg-Tg(TcraTcrb)425Cbn/J)	Jackson Labs	004194
Software and algorithms		
FlowJo version 10	FlowJo	N/A
FACS Diva	BD	N/A
GraphPad	Prism	N/A
Other		
Matrigel	Discovery Labware	08-774-552
4.0 Sutures	Ethicon	1611G
5.0 Sutures	Ethicon	8580H

RESOURCE AVAILABILITY

Lead contact

Requests for further information should be directed to and will be fulfilled by the lead contact, Ingunn M. Stromnes (ingunn@umn.edu).

Materials availability

Further information and requests for resources and reagents generated in this report should be directed to and will be fulfilled by the lead contact, Ingunn M. Stromnes (ingunn@umn.edu).

Data and code availability

- Single-cell RNA sequencing data and BulkRNA sequencing data of tumor associated macrophages have been deposited on the Gene Expression Omnibus (GEO) under the accession number GSE233068 and are publicly available.
- This paper does not report original code.
- Any additional information required to reanalyze the data reported in this paper is available from the lead contact on request.

EXPERIMENTAL MODEL AND SUBJECT DETAILS

Human samples

Human resected tumor and normal adjacent tissues were obtained from BioNET, a University of Minnesota IRB-approved protocol and tissue bank for investigators. All patients gave informed consent. Tumor and normal adjacent sample 1 were from a 74 year old white male. Tumor and normal adjacent sample 2 were from a 67 year old white female. Tumor and normal adjacent sample 3 were from a 63 year old white female. Tumor sample 4 was from a 61 year old white male.

Animals

University of Minnesota Institutional Animal Care and Use Committee (IACUC) approved all animal studies. 6- to 12-wk-old female and male C57BL/6J (000664), *Ifngr1*$^{-/-}$ (003288), *Tnfrsf1a*$^{-/-}$ (003242), *Cd40*$^{-/-}$ (002928), and *CX3CR1*^{CreER} (020940) mice were purchased from The Jackson Laboratory and on a C57Bl/6 background. Sm1x*Rag1*$^{-/-}$ mice[77], CCR2-CreER-GFP (C57BL/6-Ccr2em1(icre/ERT2)Peng/J) x I-AB-flox (B6.129X1-H2-Ab1tm1Koni/J), OT-II (B6.Cg-Tg(TcraTcrb)425Cbn/J) and *Rag*$^{-/-}$ (B6.Cg-Rag2tm1.1Cgn/J) were kindly provided by Dr. Marc Jenkins (University of Minnesota). *CCR2*^{creERT2} [C57BL/6NTac-Ccr2^{tm2982}(T2A-Cre7ESR1-T2A-mKate2)] reporter mice[76] were kindly provided by Burkhart Becker (University of Zurich) and were crossed to R26-tdTomato reporter mice (B6.Cg-Gt(ROSA)26Sor$^{tm9(CAG-tdTomato)Hze}$/J). Animals were maintained in SPF conditions at the University of Minnesota Research Animals Resources facility with free access to food and water and kept on a 12-hour light-dark cycle.

Tumor cell lines

The *KPC*2a cell line was transduced to express click beetle red luciferase linked to eGFP (CB-eGFP)[30]. Tumor cells were cultured in Basic media: DMEM (Life Technologies) + 10% FBS (Life Technologies) + 2.5 mg/ml amphotericin B (Life Technologies) + 100 mg/ml penicillin/streptomycin (Life Technologies) + 2.5 g dextrose (Fisher Chemical) at 37C + 5% CO_2. Medium was sterile filtered and stored in the dark at 4C. Cell lines used for experiments were maintained below passage 15 and 0.25% trypsin-EDTA (Thermo Fisher) was used for cell passage.

METHOD DETAILS

Orthotopic tumor cell implantation

For orthotopic tumor implantation, mice received 1 mg/kg slow-release buprenorphine injected subcutaneously prior to surgery for analgesia. Mice were anesthetized using continuous flow of 2-5% isoflurane. Hair was removed using clippers and Nair (Church & Dwight Co., Inc.) and the abdomen was sterilized using a series of 100% EtOH and Betadine washes. Once mice reached surgical plane anesthesia, a small incision was made in the abdomen followed by a small incision in the peritoneum to access the pancreas. 1x10^5 *KPC2a* cells in 20 μl of 60% Matrigel (Discovery Labware) were injected into the pancreas using an insulin syringe (Covidien)[30]. Sutures were used to close the peritoneum (Ethicon) and skin was closed using wound clips (CellPoint Scientific). Mice were monitored daily for 5 days to ensure healing of outer skin.

Tamoxifen administration

For fate mapping studies, Ccr2 reporter mice were gavaged orally with 250 μl of Tamoxifen (Sigma Aldrich Cat: T5648) at 20 mg ml−1 in corn oil on the day of tumor implantation or 1 day prior to tumor implantation or as indicated.

In vivo antibody treatments

For T cell depletion studies, mice were injected intraperitoneally (I.P.) with 200 μg of either anti-CD4 (BioXcell, Cat#-BE0003-1) or anti-CD8 (BioXcell, Cat#-BE0061) on days -1, +2 and +10 post tumor implantation. For CD40L blockade experiments, 500 μg of anti-CD40L (BioXcell, Cat#-BP0017-1) was injected I.P. on days -1 and +2 post tumor implantation.

Preparation of mononuclear cells from tissues

Spleens were mechanically dissociated to single cells followed by RBC lysis in 1 ml of Tris-ammonium chloride (ACK) lysis buffer (Life Technologies) for 2 min at room temperature (rt). RBC lysis was quenched by addition of 9 ml of T cell media. Splenocytes were centrifuged at 1400 rpm for 5 min, resuspended in T cell media (DMEM, 10% FBS, 2 μM L-glutamine, 100 U/ml penicillin/streptomycin, 25 μM 2-β-mercaptoethanol) and kept on ice until further analysis. Tumors were collagenase digested at 37°C for 15 minutes then mechanically digested to single cell suspensions and washed twice to remove cell debris and pancreatic enzymes.

Cell surface staining

Cells were stained in the presence of 1:500 Fc block (CD16/32, Tonbo) and antibodies diluted 1:200 in FACs buffer (PBS+2.5% FBS) for 45 minutes in the dark at 4°C. Ghost viability dye BV540 (Tonbo) was used to exclude dead cells at 1:500. Cells were fixed in 2% PFA or fixation buffer (Tonbo) for 10-15 at room temperature in the dark prior to data acquisition. Cells were acquired within 24 h using a Cytek Aurora.

Intracellular staining

The Foxp3 intracellular staining kit (Tonbo) was used for detecting intracellular transcription factors and proteins. Following cell surface staining, cells were washed 2X in FACs buffer, fixed for 30 min at 4°C, washed 2X in permeabilization buffer, stained with antibodies diluted 1:100 in permeabilization buffer for 1-2 hours in the dark at 4°C. Cells were washed 2X in permeabilization buffer, resuspended in FACs buffer and acquired within 24 h on a Cytek Aurora flow cytometer following addition of cell counting beads (Sigma).

PMA/Ionomycin restimulation

To determine *ex vivo* T cell functionality from tumor-bearing mice, single cell suspensions from spleen and tumor were obtained and activated *in vitro*[30]. Briefly, mononuclear cells were restimulated with 1X Cell Stimulation Cocktail (eBioscience) in the presence of Golgiplug and Golgistop (BD) according to manufacturer's instructions in T cell media. 4-5 hours later, cells were stained with live/dead ghost dye at 1:500 (Tonbo) and the following antibodies at diluted in FACs buffer at 1:200 against CD45 (30F-11, BD), CD3 (17A2, Biolegend), CD4 (RM4.5, Tonbo), CD8 (53-6.7, Tonbo), Klrg1 (2F1, eBioscience), and CD44 (IM7, Tonbo) for 30 minutes at 4°C in the dark. Cells were washed 2X in FACs buffer, fixed/permeabilized using the BD cytofix/cytoperm kit (BD) and stained with anti-IFNγ (XMG1.2, Biolegend) diluted 1:100 in perm/wash buffer for 1 h at 4°C. Cells were washed 2X in perm/wash buffer, resuspended in FACs buffer and stored overnight at 4°C in the dark. Cells were acquired the following day on a Fortessa 1770 flow cytometer following the addition of counting beads (Sigma) and analyzed using FlowJo software (version 10).

Murine tumor scRNAseq sample acquisition and data analysis

For scRNAseq, 4 tumors from each group were harvested and processed to generate single cell suspensions. Live CD45+ Tomato+ cells and CD45+ Tomato- cells were FACS sorted using a BD FACSAria II. Each population was then stained with hashtag oligo antibodies (BD Biosciences; HTO#9 and HTO#10) and BD Bioscience CITEseq antibodies: CD274 (Cat:153604), IA-IE (Cat:107653), CD11b (Cat: 101265), Folate receptor beta (Cat: 153307) for 30 mins at 4°C (1:500) then recombined at a 1:1 mix. Sorted cells were resuspended in a final concentration of 100 cells per μl in 1X PBS containing 0.04% BSA for single cell capture of approximately 20,000 cells per group. Cells were submitted to University of Minnesota Genomics Core (UMGC) for single cell 10X Chromium 3' GEX Capture and NovaSeq 2 x150 S4 sequencing targeting ~50,000 reads per cell.

For preprocessing of the mouse scRNAseq data, we removed genes detected in less than 10 cells, potential empty cells with less than 200 feature counts, and apoptotic cells possessing more than 25% mitochondrial mRNA content. We then utilized DoubletFinder[78] to perform a more elegant doublet removal independently for each sequence capture prior to data merging and integration. NormalizeData and ScaleData functions from Seurat (v4.0.1) were used for normalization and scaling. Variable features were extracted using FindVaribleFeatures function. For integration purpose, we chose Harmony package[79]. The first 20 principle components were used to generate uniform manifold approximation and projection (UMAP) and t-distributed stochastic neighbor embedding (tSNE). For gene set scores, Seurat AddModuleScore function was used, where pro-inflammatory (*H2-Aa, Cxcl9, Il1b, Cxcl10, Tnf*) and anti-inflammatory (*Mrc1, Il10, Siglec1, FRβ, Arg1*) gene sets were used. SingleR (v1.6.1)[80] was used as an unbiased computational method for immune cell type annotation. Clusters generated using resolution 0.1 that were identified as SingleR monocyte and macrophage were extracted for further sub-clustering, pseudo-time trajectory and intercellular interaction analysis. Trajectory analysis were performed with support of Monocle3 (v1.0.0)[41]. In order to avoid batch effects across captures, we applied "harmony" as the base reduction method for all Monocle3 functions. Cells in the monocyte cluster were used as the root population to calculate pseudo-time inference of monocyte-macrophage differentiation. Pseudo-time parameter from ordered cells was extracted for

visualization in "harmony" embeddings. For intercellular communication analysis, we utilized NicheNet (v1.0.0)[42]. All NicheNet models were first converted to mouse gene symbols using convert_human_to_mouse_symbols function.

Bulk RNA sequencing collection and analysis

Tumor single cell suspensions were isolated from 4 WT and 4 *Ifngr1*-/- mice and CD45+ CD11b+ F4/80+ MHCII^{hi} and MHCII^{lo} macrophages were FACS sorted into Trizol for RNA extraction. A minimum of 10,000 cells were sorted and submitted to UMGC for RNA isolation and sequencing using the Novaseq platform. Bulk RNAseq processing was performed using CHURP pipeline developed by the Minnesota Supercomputing Institute, which implemented and integrated Trimmomatic, HISAT2, SAMTools and featureCounts. Mus musculus GRCm38 (Ensembl release 102) was used as mouse reference genome. Differential expression analysis was adopted from DEseq2 (v.1.32.0). Pathway analyses were performed using fgsea function from the fgsea package (v.1.18.0).

Human PDA samples

De-identified and resected human tumor and normal adjacent tissues were obtained from BioNET, a University of Minnesota IRB-approved protocol and tissue bank for investigators. Tumors were from patients diagnosed with PDA. Mononuclear cells were stored at -80°C in Cryostor and thawed for staining and flow cytometric analysis like mouse samples.

Human PDA scRNAseq data analysis

Publicly available scRNAseq data from tumors from 6 PDA patients available from Elyada et al[51] was downloaded after NIH approval at dbGaP (accession number phs001840.v1.p1). Filtered count matrices for 6 human tumor samples (SRR9274536, SRR9274537, SRR9274538, SRR9274539, SRR9274542, SRR9274544) were used as input data. Analytic tools used for human PDA scRNAseq data were identical to that of mouse scRNAseq described above, with the exception that SingleR model training was performed using HumanPrimaryCellAtlasData from Celldex.

QUANTIFICATION AND STATISTICAL ANALYSIS

Statistical analyses were performed using GraphPad software (version 9.0). Mouse experiments include n=3-8 mice per group. Unpaired, two-tailed Student's T test was used to compare two-group data. One-way ANOVA and Tukey posttest were used for comparing >2-group data. Data are presented as mean ± standard error of the mean (SEM), and $p<0.05$ was considered significant. *$p<0.05$, **$p<0.005$, ***$p<0.0005$, and ****$p<0.0001$.

Cell Reports, Volume *42*

Supplemental information

Tumor-specific CD4 T cells instruct monocyte fate in pancreatic ductal adenocarcinoma

Michael T. Patterson, Adam L. Burrack, Yingzheng Xu, Grant H. Hickok, Zoe C. Schmiechen, Samuel Becker, Eduardo Cruz-Hinojoza, Patricia R. Schrank, Ainsley E. Kennedy, Maria M. Firulyova, Ebony A. Miller, Konstantin Zaitsev, Jesse W. Williams, and Ingunn M. Stromnes

Supplemental Figure 1

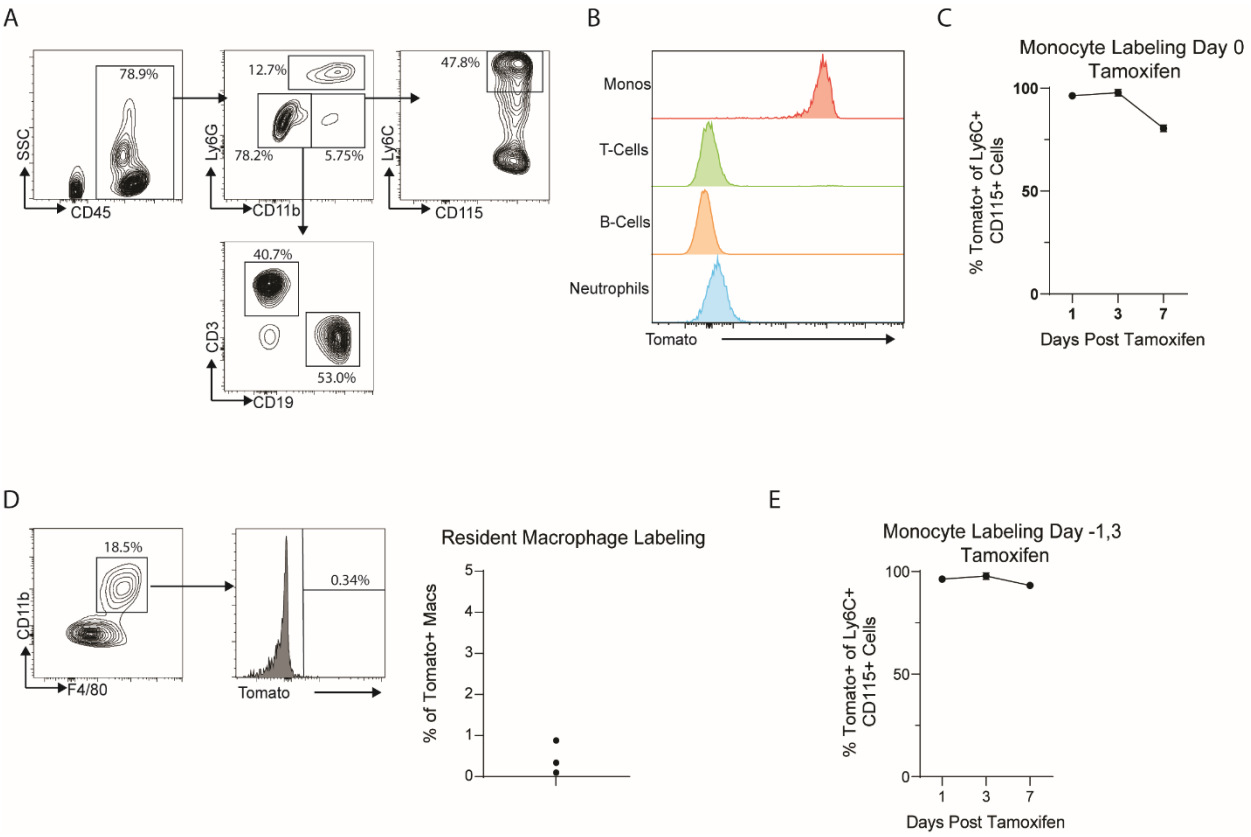

Supplemental Figure 1. Labeling efficiency of monocytes in CCR2^{CreER} R26^{TdTomato} fate mapping mice. Related to Figure 1.

A) Gating strategy for analysis of circulating immune cells from tumor bearing CCR2^{CreER} R26^{TdTomato} mice 1 day post tamoxifen administration.

B) Tomato reporter expression by circulating immune subsets from tumor bearing CCR2^{CreER} R26^{TdTomato} mice 1 day post tamoxifen administration.

C) Proportion of circulating Tomato+ monocytes from tumor bearing CCR2^{CreER} R26^{TdTomato} mice treated with tamoxifen on the day of tumor implantation (Day 0, n=4 mice per group). Data are mean ± S.E.M.

D) Labeling and quantification of pancreatic resident (Tomato-) macrophages from non-tumor bearing CCR2^{CreER} R26^{TdTomato} 1 day post tamoxifen administration. CD11b+F480+ macrophages were gated on live, CD45+Ly6G- cells.

E) Proportion of circulating monocytes that are Tomato+ from tumor bearing CCR2^{CreER} R26^{TdTomato} treated with tamoxifen 1 day prior to tumor implantation (Day -1) and on day 3 after tumor implantation (n=4 mice per timepoint).

Supplemental Figure 2

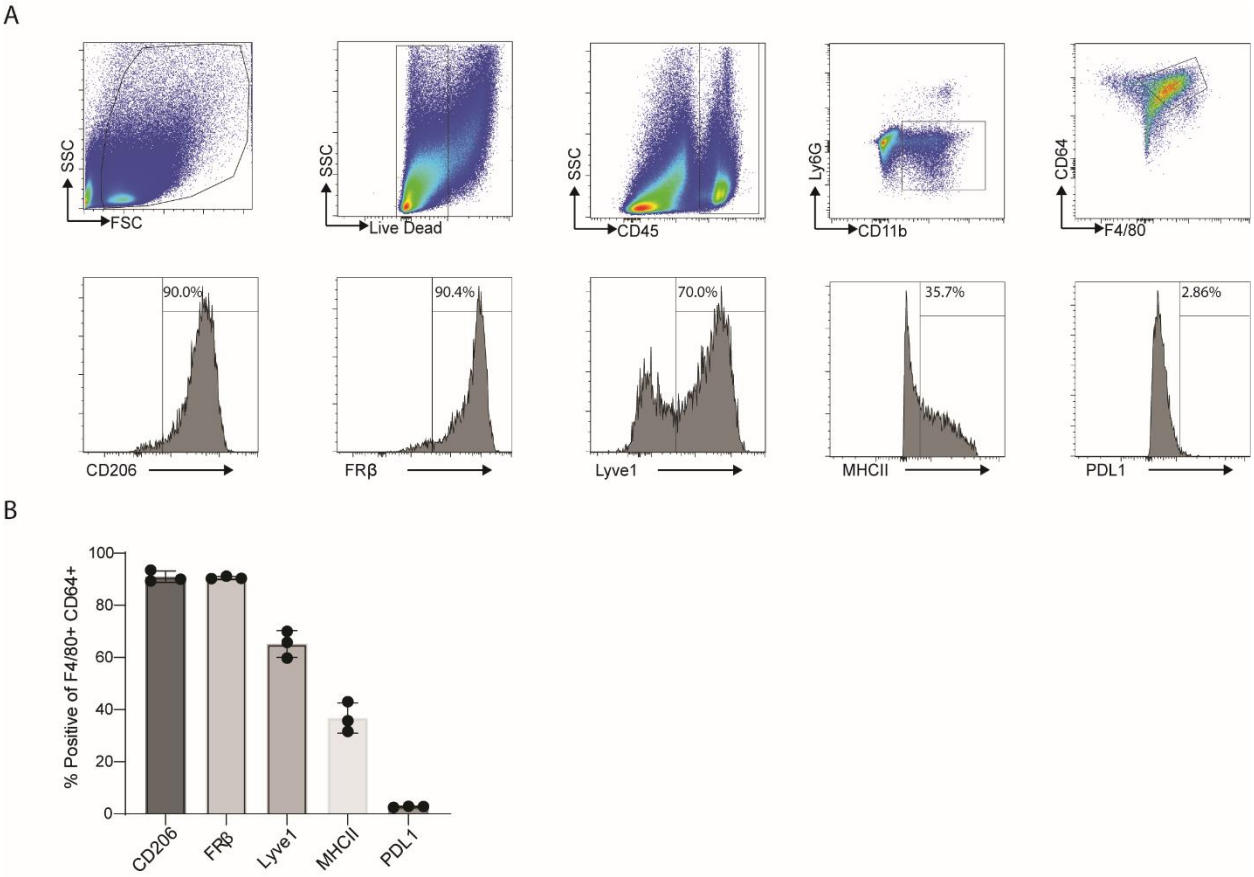

Supplemental Figure 2. Phenotyping of steady state pancreatic resident macrophages. Related to Figure 1M-O.

A) Gating strategy for analysis of pancreatic macrophages from untreated non-tumor bearing CCR2^{CreER} R26^{TdTomato} mice. Live cells are gated off single cells.

B) Proportion of CD64+F4/80+ pancreatic macrophages that express the indicated marker (n=3). Each dot is an independent mouse. Data are mean ± S.E.M.

Supplemental Figure 3

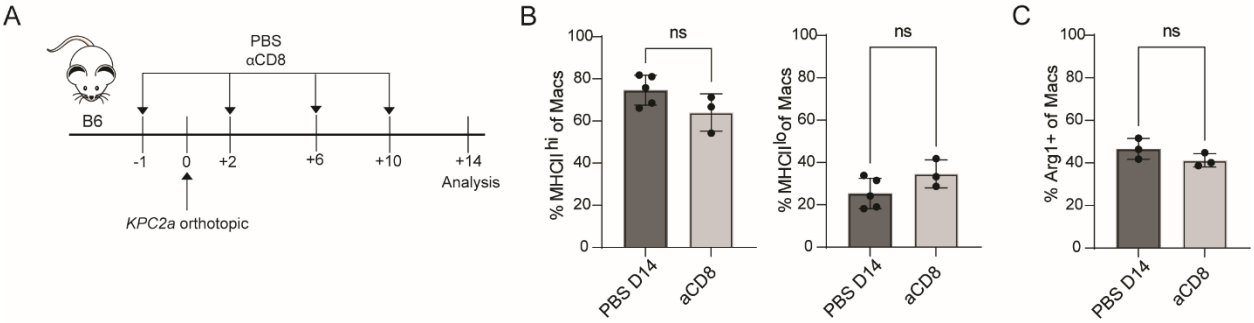

Supplemental Figure 3. Prolonged CD8 T cell depletion does not change macrophage phenotype. Related to Figure 2 A-K.

A) Schematic for testing the impact of CD8 T cells on macrophage phenotype.

B) $MHCII^{hi}$ or $MHCII^{lo}$ macrophage frequency from tumors isolated from PBS or αCD8 treated mice at 14 days after tumor implantation (n=3-4 mice per group). Populations are gated on CD64+ F4/80+ cells. Each dot is an independent mouse. Data are mean ± S.E.M.

C) Arg1+ macrophage frequency from tumors isolated from PBS or αCD8 treated mice at 14 days after tumor implantation (n=3-4 mice per group). Populations are gated on CD64+ F4/80+ cells. Each dot is an independent mouse. Data are mean ± S.E.M.

Supplemental Figure 4

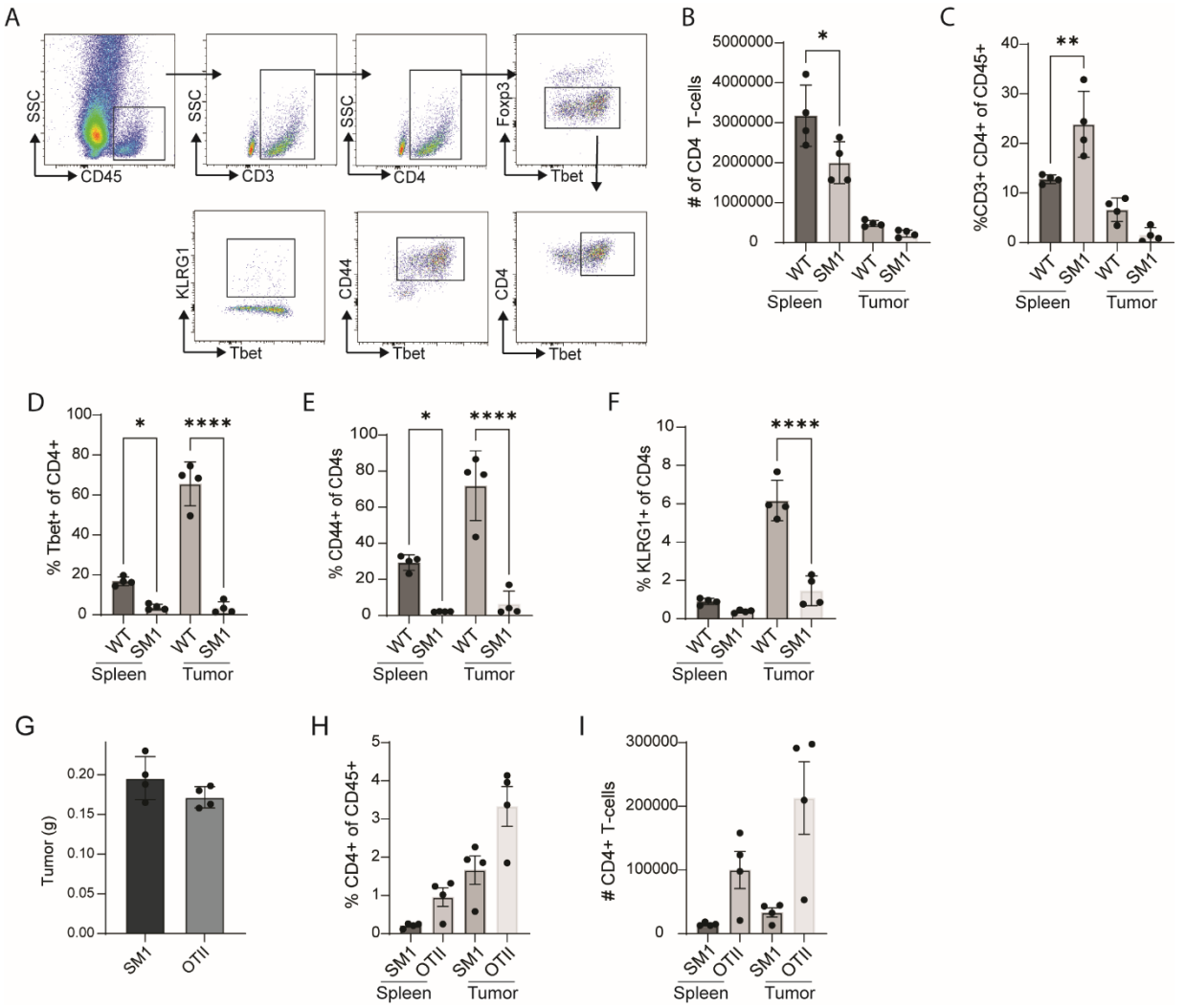

Supplemental Figure 4. Impact of tumor antigen specificity on intratumoral CD4 T cell quantity and phenotype. Related to Figure 2L-T.

A) Gating strategy for CD4 T cells on day 7 post orthotopic tumor implantation. Representative plots are from WT mouse at day 7 post tumor and gated on live, single cells.

B-C) CD4+T cell number (B) or frequency (C) from WT or SM1 *Rag1-/-* mice at day 7 post tumor implantation (n=4 per group). Each dot is an independent mouse. Data are mean ± S.E.M. **p*<0.05, Student's t-test for each tissue.

D-F) Proportion of CD4+Foxp3- (Tcons) T cells that express Tbet (**D**), CD44 €, or KLRG1 (**F**) in WT or SM1 *Rag1-/-* mice at day 7 post tumor implantation (n=4 per group). Each dot is an independent mouse. Data are mean ± S.E.M. **p*<0.05, ***p*<0.005, *****p*<0.0001, Student's t-test for each tissue.

G) Tumor weight in grams from Figure 2Q. Data are mean ± S.E.M. n=4 mice per group.

H-I) CD4+T cell number or frequency from KPC-OVA tumor bearing recipients of SM1 *Rag1-/-* or OTII CD4 T cells at day 7 post tumor implantation (n=4 per group). Each dot is an independent mouse. Data are mean ± S.E.M. **p*<0.05, Student's t-test for each tissue.

Supplemental Figure 5

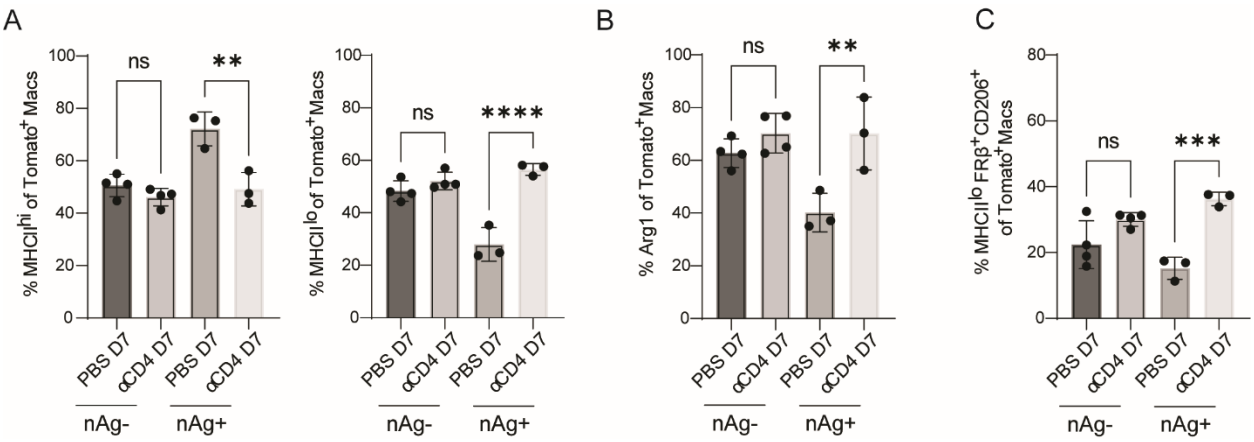

Supplemental Figure 5. Impact of tumor neoantigen expression on macrophage phenotype. Related to Figure 2.

A) Intratumoral MHCII^{hi} or MHCII^{lo} macrophage frequency from tamoxifen treated CCR2^{CreER} R26^{tdTomato} mice bearing CB neoantigen expressing (nAg+) or CB negative (nAg-) tumors 7 days after implantation (n=3-4 mice per group). CD4 T cell depletion was performed as in Figure 2. Populations are gated on CD64+ F4/80+ cells. Each dot is an independent mouse. Data are mean ± S.E.M.

B) Arg1+ macrophage frequency from tumors isolated from nAg+ and nAg- tumors 7 days after implantation (n=3-4 mice per group). Populations are gated on CD64+ F4/80+ cells. Each dot is an independent mouse. Data are mean ± S.E.M.

C) Intratumoral MHCII^{lo} CD206+ FRβ+ macrophage frequency from from mice in A. Populations are gated on CD64+ F4/80+ cells. Data are mean ± S.E.M.

Supplemental Figure 6

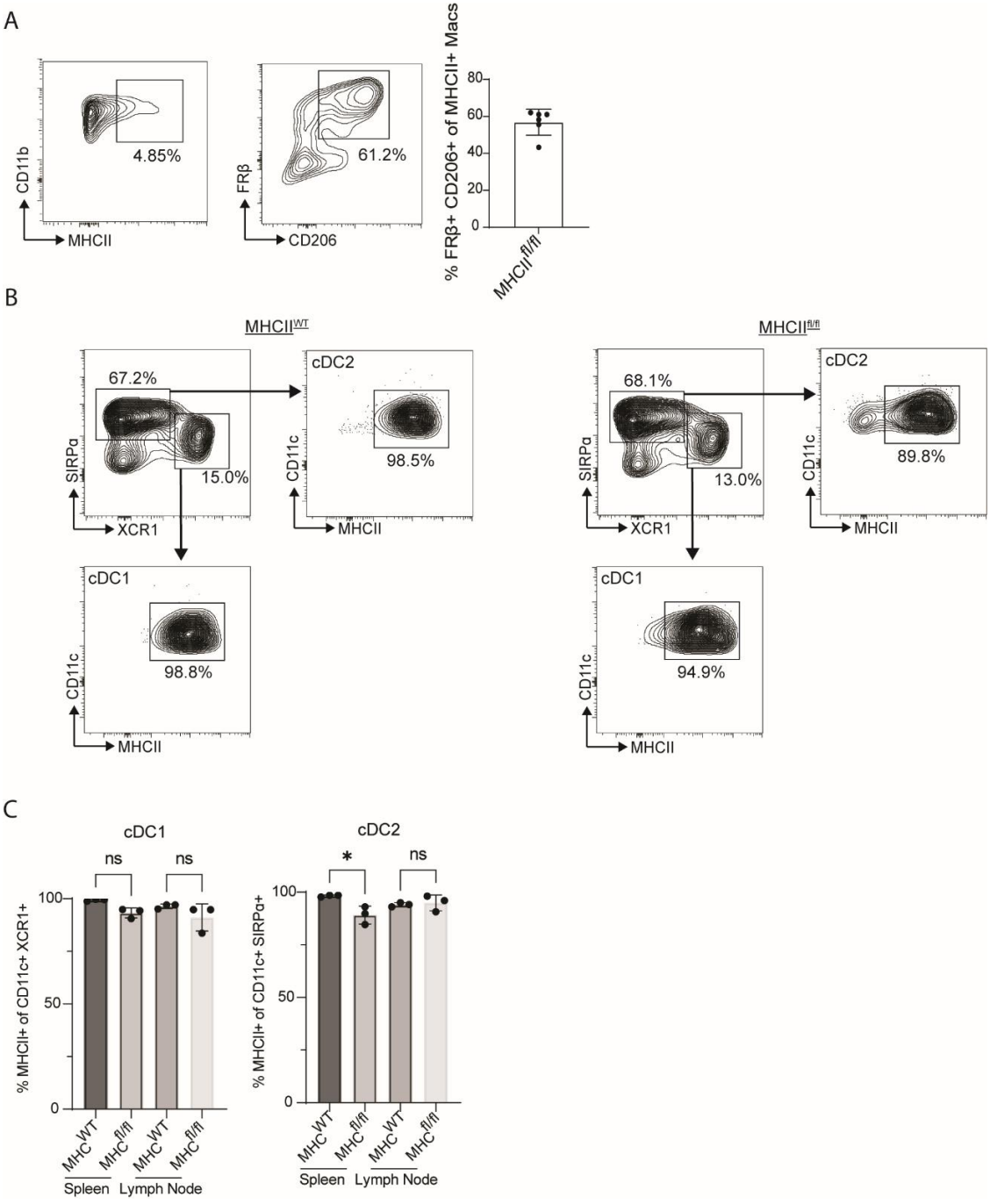

Supplemental Figure 6. MHCII is retained on tissue resident macrophages and dendritic cells from CCR2^{CreER} MHCII$^{flox/flox}$ tumor bearing mice. Related to Figure 3.

A) Phenotype of remaining intratumoral MHCII^{hi} macrophages from CCR2^{CreER} MHCII$^{flox/flox}$ tumor bearing mice treated with tamoxifen as in Figure 3 (n=6 mice). Data are mean ± S.E.M.

B) Gating of splenic and lymph node DC subsets from CCR2^{CreER} MHCII$^{flox/flox}$ and MHCII^{WT} mice treated with 2 doses of tamoxifen on days 0 and 4 and analyzed on day 5 (n=3 mice per group).

C) Proportion of cDC1 and cDC2 cells that express MHCII from mice in B. Data are mean ± S.E.M.

Supplemental Figure 7

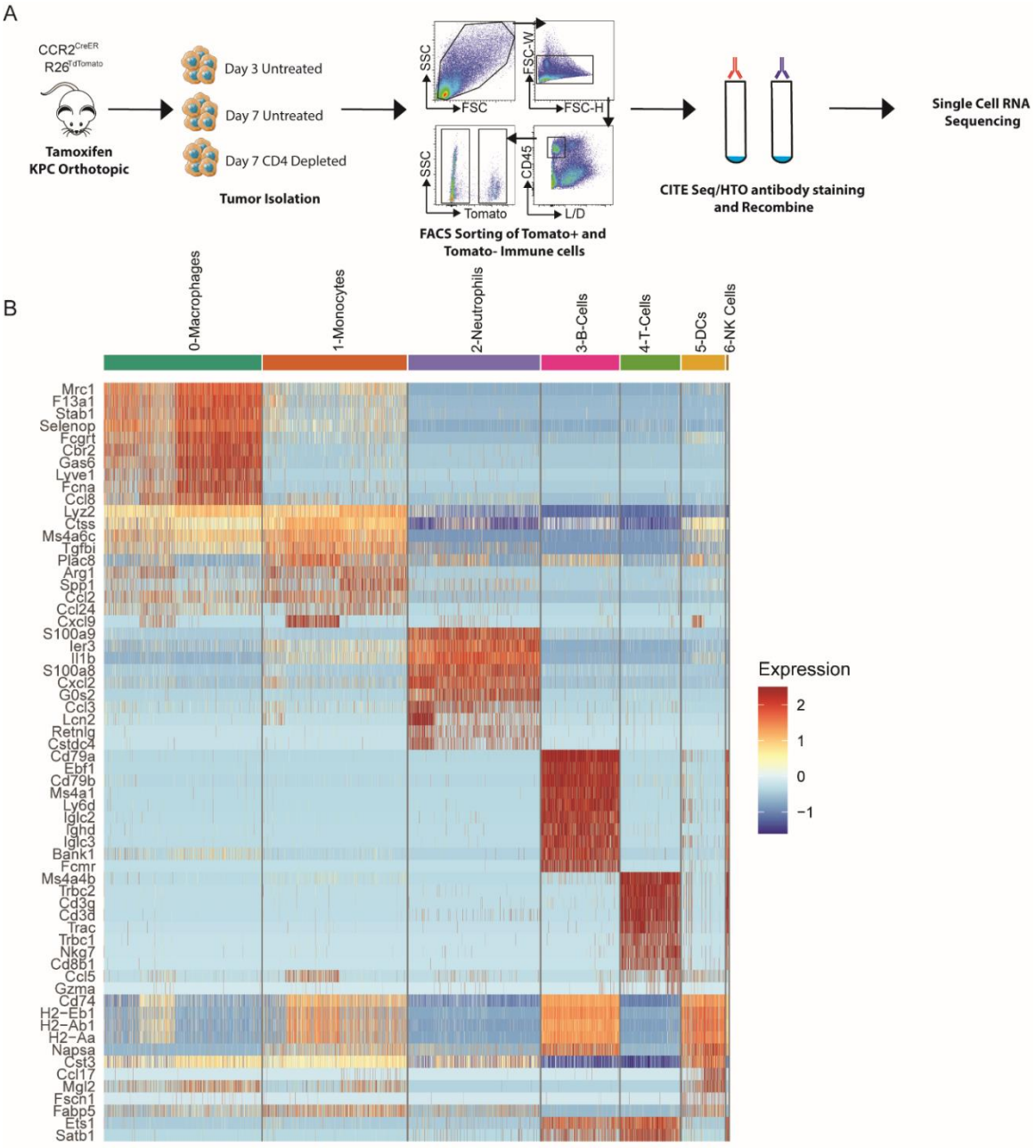

Supplemental Figure 7. scRNAseq analysis of immune cells in monocyte-fate mapping tumor-bearing mice. Related to Figure 4.

A) Experimental approach for scRNAseq analysis. CCR2^{CreER} R26^{TdTomato} mice were orthotopically implanted with *KPC*2a tumors. One cohort was treated with anti-CD4 at day -1 and day +2. All cohorts were administered tamoxifen on the day of tumor implantation. Tumors were isolated from a total of 4 mice per cohort per timepoint. Tumors from mice treated with anti-CD4 were harvested on day 7. Intratumoral Tomato+ and Tomato- cells were FACS sorted, labeled with CITE-Seq antibodies, hash tagged and pooled at a 1:1 mixture for scRNAseq.
B) Heatmap showing top 5 differentially expressed genes for each cluster. singleR was used to name cell populations based on top differentially expressed genes.

Supplemental Figure 8

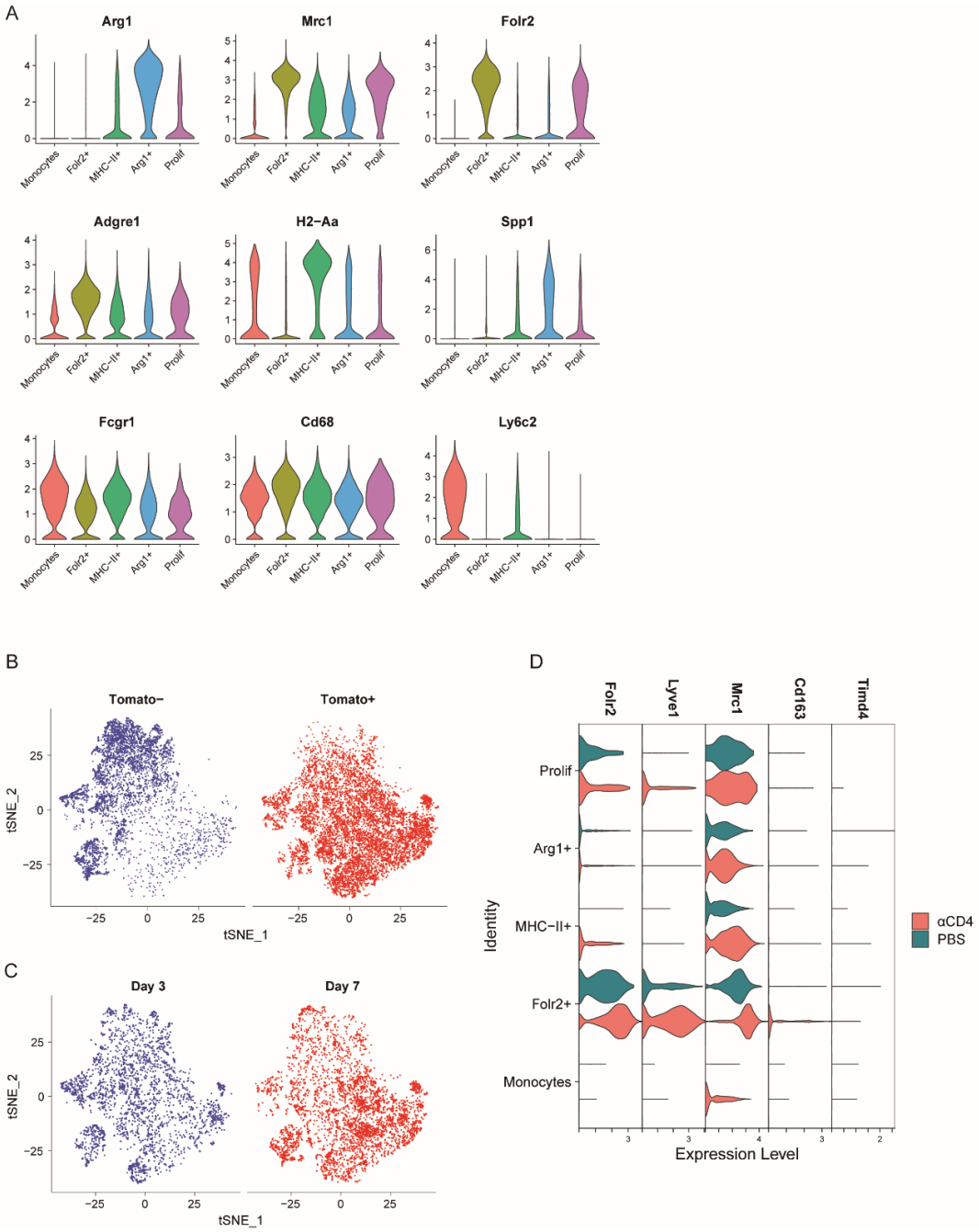

Supplemental Figure 8. Monocyte/macrophage gene changes following CD4 T cell depletion. Related to Figure 4 and Figure 5.

A) Violin plots of selected cluster defining genes from scRNAseq data.
B) tSNE plots of Tomato+ and Tomato- cells from PBS control mice merged from days 3 and 7.
C) tSNE plots of monocyte/macrophage clusters from PBS control mice merged from days 3 and 7.
D) Violin plots of selected genes associated with a tissue resident phenotype.

Supplemental Figure 9

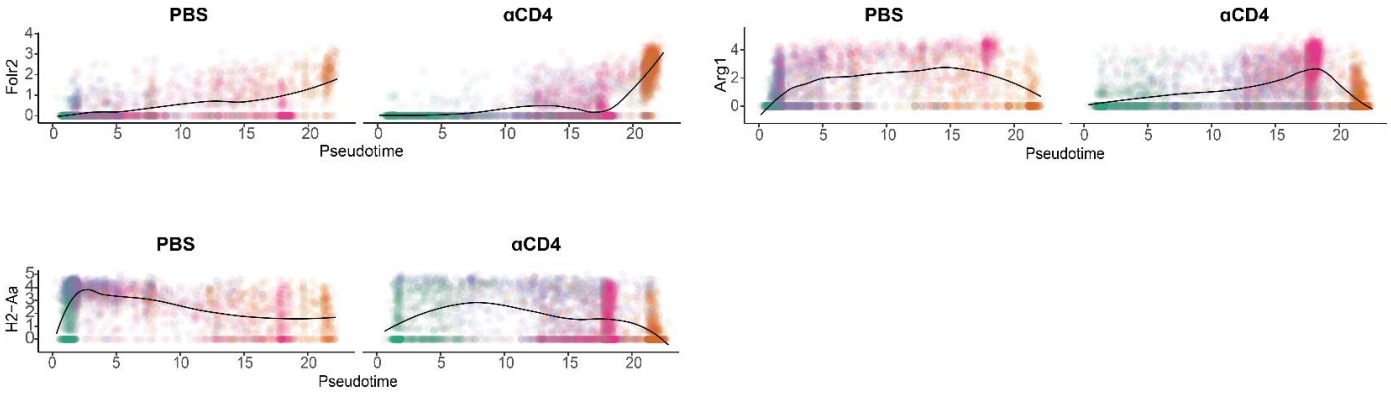

Supplemental Figure 9. Kinetic analysis of cluster defining genes. Related to Figure 5. Kinetic analysis of cluster defining gene expression over pseudotime. Folr2 defines Folr2+ cluster, MHCII defines MHCII+ cluster and Arg1 defines Arg1+ cluster.

Supplemental Figure 10

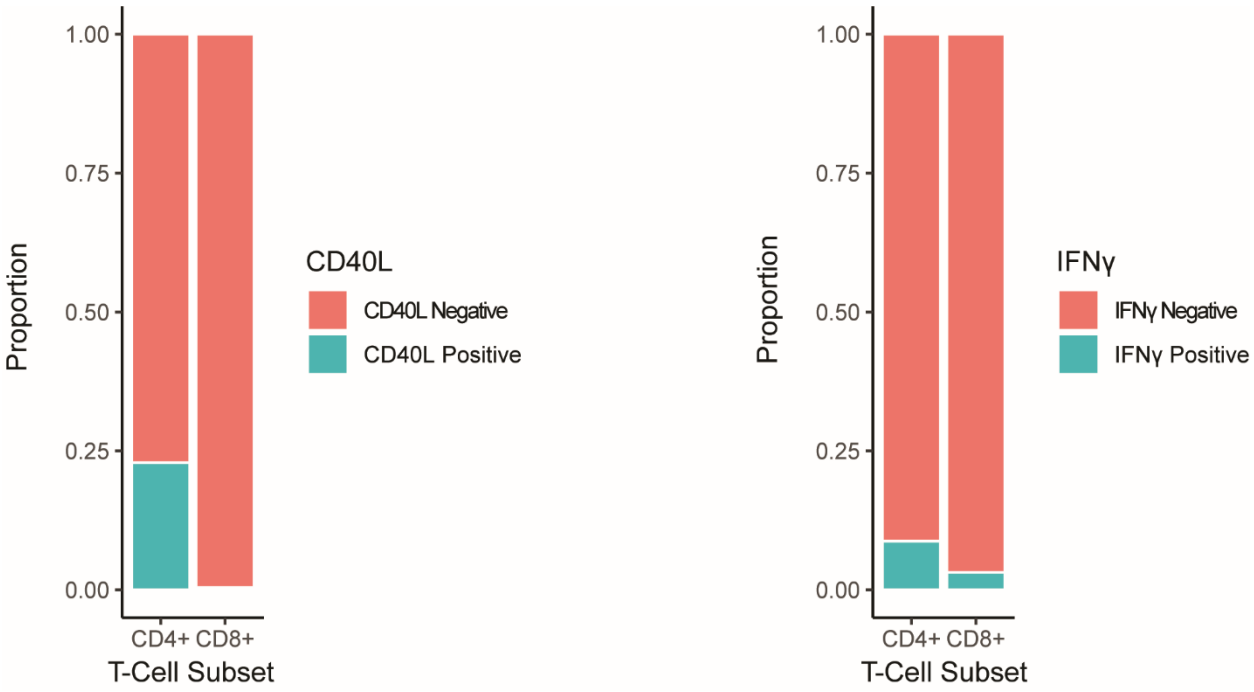

Supplemental Figure 10. Intratumoral CD4 and CD8 T cell *Ifng* or *Cd40l* **expression from Day 7 scRNAseq data. Related to Figure 6.** Proportion of CD4 and CD8 T cells that express *Ifng* or *Cd40l* was determined by scRNAseq analysis of intratumoral T cell clusters from day 7 tumors.

Supplemental Figure 11

Supplemental Figure 11. Bulk RNA sequencing of TAMs from *Ifngr1-/-* and WT mice. Related to Figure 6H-I. A) FACS sorting strategy for isolation of MHCII^{hi} and MHCII^{lo} TAMS from 4 pooled WT and 4 pooled IFNyR KO mice on 14 days post tumor implantation.
B) Heat map of top 50 differentially expressed genes for each macrophage population.

Supplemental Figure 12

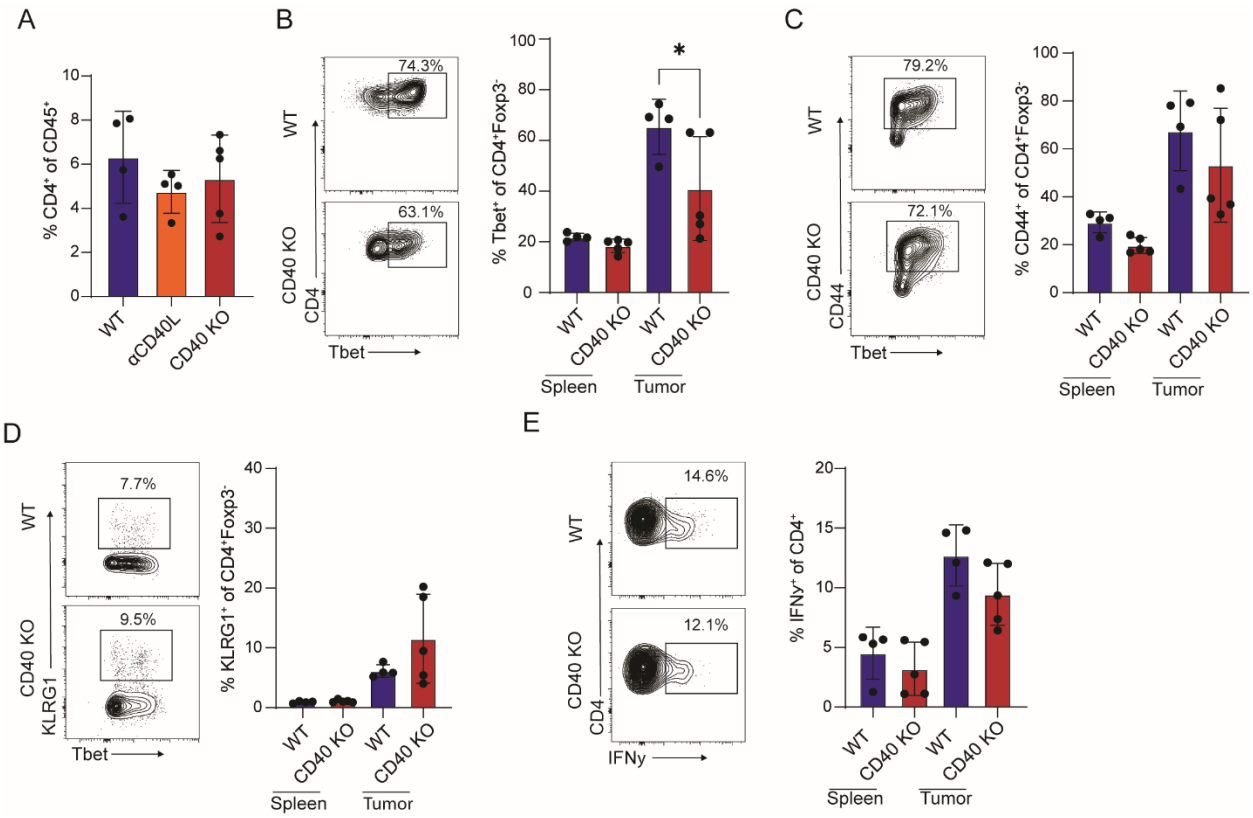

Supplemental Figure 12. Impact of CD40 deletion or CD40L blockade on T cell phenotype. Related to Figure 6J-M.

A) Proportion of CD4+ T cells among intratumoral CD45+ immune cells from tumors of Day 7 WT, CD40 KO and CD40L treated mice. Each dot is an independent mouse. Data are mean ± S.E.M. n=4-5 mice per group.

B) Representative plots and proportion of CD4+Foxp3- T cells that express T-bet from mice in A. Each dot is an independent mouse. Data are mean ± S.E.M. n=4-5 mice per group. *p<0.05, Student's t-test for each tissue.

C) Representative plots and proportion of CD4+Foxp3- T cells that express CD44 from mice in A. Each dot is an independent mouse. Data are mean ± S.E.M. n=4-5 mice per group.

D) Representative plots and proportion of CD4+Foxp3- T cells that express Klrg1 from mice in A. Each dot is an independent mouse. Data are mean ± S.E.M. n=4-5 mice per group.

E) Representative plots and proportion of CD4+ T cells that are producing IFNy following PMA/Ionomycin treatment. Each dot is an independent mouse. Data are mean ± S.E.M. n=4-5 mice per group

Supplemental Figure 13

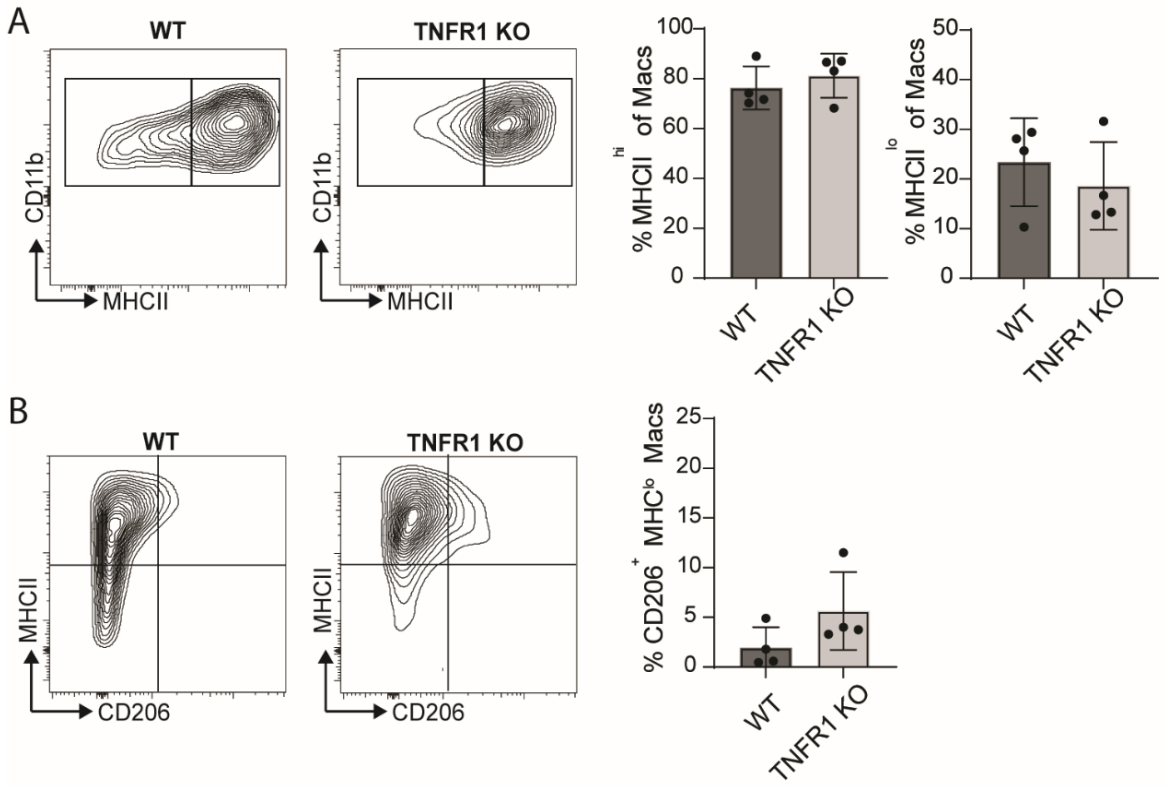

Supplemental Figure 13. Impact of host cell Tnfr1 deletion on macrophage phenotype. Related to Figure 6.

A) MHCII^{hi} and MHCII^{lo} macrophage frequency from tumors isolated from WT and *Tnfr1-/-* mice 7 days after implantation (n=4 mice per group). Populations are gated on CD64+ F4/80+ cells. Each dot is an independent mouse. Data are mean ± S.E.M.

B) MHCII^{lo} CD206+ macrophage frequency in tumors from WT and *Tnfr1-/-* mice in A. Populations are gated on CD64+ F4/80+ cells. Each dot is an independent mouse. Data are mean ± S.E.M.

Supplemental Figure 14

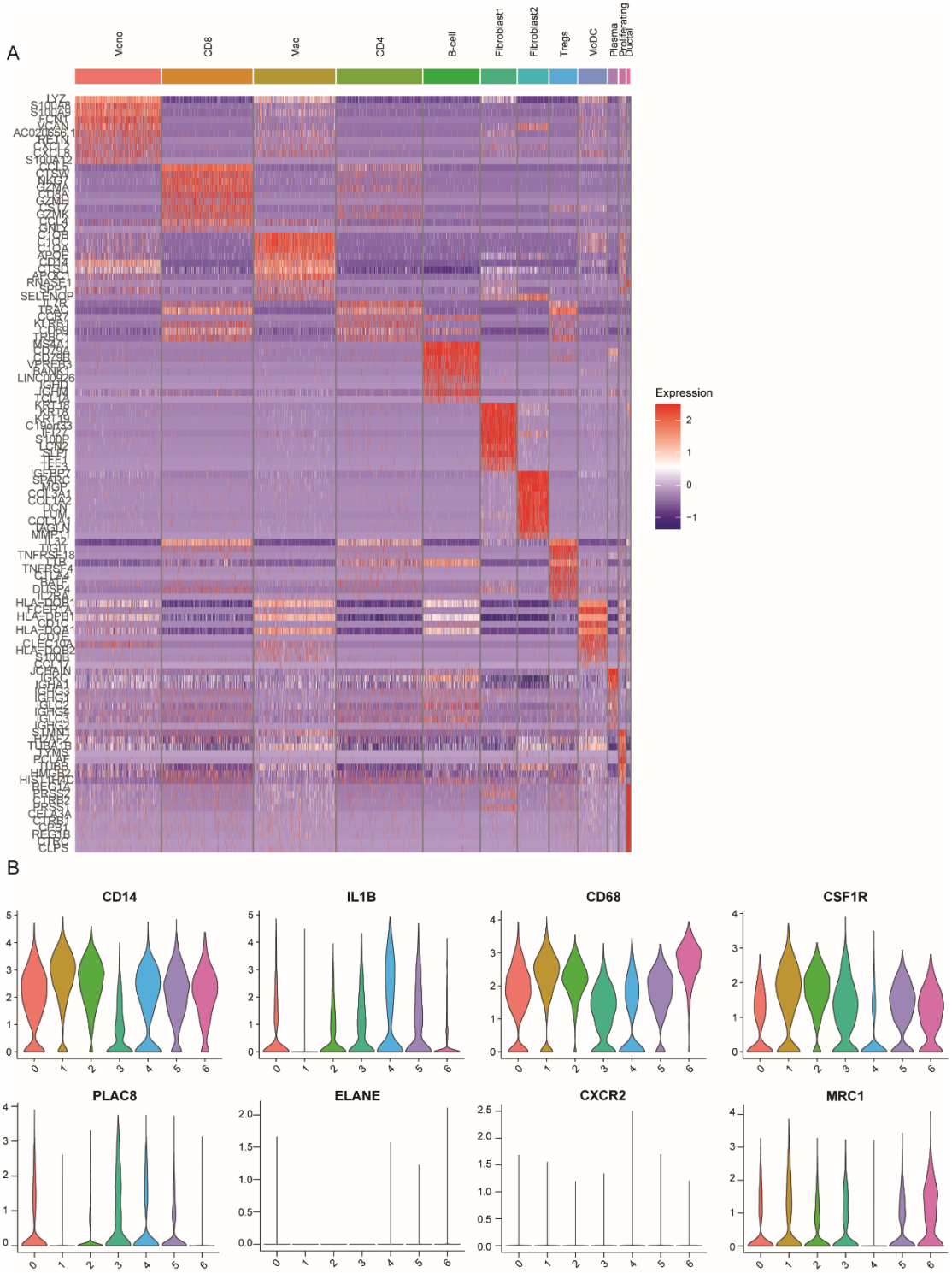

Supplemental Figure 14. Human PDA scRNAseq analysis. Related to Figure 7.
A) Heatmap of top differentially expressed genes from 6 resected human PDAs from Elyada *et al*. Cell populations were clustered in the UMAP space and named based off top differentially expressed genes
B) Violin plots of selected cluster defining genes from A.